Neurobiology of Disease

Arcuate Nucleus Overexpression of NHLH2 Reduces Body Mass and Attenuates Obesity-Associated Anxiety/Depression-like Behavior

Rodrigo S. Carraro,[1] Guilherme A. Nogueira,[1] Davi Sidarta-Oliveira,[1] Rodrigo S. Gaspar,[1] Nathalia R. Dragano,[1] Joseane Morari,[1] Vanessa C. D. Bobbo,[1] Eliana P. Araujo,[1] Natalia F. Mendes,[1] Ariane M. Zanesco,[1] Natalia Tobar,[2] Celso D. Ramos,[2] Jéssica M. Toscaro,[3] Marcio C. Bajgelman,[3] and Licio A. Velloso[1,4]

[1]Laboratory of Cell Signaling, Obesity and Comorbidities Research Center, University of Campinas, Campinas, 13083-970, Sao Paulo, Brazil, [2]Nuclear Medicine Service, Department of Radiology, Hospital of Clinics, University of Campinas, Campinas, 13083-970, Sao Paulo, Brazil, [3]Brazilian Center for Research in Energy and Materials, Brazilian Biosciences National Laboratory, Campinas, 13083-970, Sao Paulo, Brazil, and [4]National Institute of Science and Technology, Neuroimmunomodulation. Fiocruz, 21040-900, Rio de Janeiro, Brazil

Nescient helix-loop-helix 2 (NHLH2) is a hypothalamic transcription factor that controls the expression of prohormone convertase 1/3, therefore having an impact on the processing of proopiomelanocortin and thus on energy homeostasis. Studies have shown that KO of *Nhlh2* results in increased body mass, reduced physical activity, and hypogonadism. In humans, a polymorphism of the *NHLH2* gene is associated with obesity; and in Prader–Willi syndrome, a condition characterized by obesity, hypogonadism and behavioral abnormalities, the expression of NHLH2 is reduced. Despite clinical and experimental evidence suggesting that NHLH2 could be a good target for the treatment of obesity, no previous study has evaluated the impact of NHLH2 overexpression in obesity. Here, in mice fed a high-fat diet introduced right after the arcuate nucleus intracerebroventricular injection of a lentivirus that promoted 40% increase in NHLH2, there was prevention of the development of obesity by a mechanism dependent on the reduction of caloric intake. When hypothalamic overexpression of NHLH2 was induced in previously obese mice, the beneficial impact on obesity-associated phenotype was even greater; thus, there was an 80% attenuation in body mass gain, reduced whole-body adiposity, increased brown adipose tissue temperature, reduced hypothalamic inflammation, and reduced liver steatosis. In this setting, the beneficial impact of hypothalamic overexpression of NHLH2 was a result of combined effects on caloric intake, energy expenditure, and physical activity. Moreover, the hypothalamic overexpression of NHLH2 reduced obesity-associated anxiety/depression behavior. Thus, we provide an experimental proof of concept supporting that hypothalamic NHLH2 is a good target for the treatment of obesity.

Key words: energy expenditure; food intake; insulin; leptin

Significance Statement

Obesity is a highly prevalent medical condition that lacks an effective treatment. The main advance provided by this study is the demonstration of the beneficial metabolic and behavioral outcomes resulting from the overexpression of NHLH2 in the hypothalamus. When NHLH2 was overexpressed simultaneously with the introduction of a high-fat diet, there was prevention of obesity by a mechanism dependent on reduced caloric intake. Conversely, when NHLH2 was overexpressed in previously obese mice, there was reduction of the obese phenotype because of a combination of reduced caloric intake, increased physical activity, and increased thermogenesis. In addition, the overexpression of NHLH2 reduced anxiety/depression-like behavior. Thus, NHLH2 emerges as a potential target for the combined treatment of obesity and its associated anxiety/depression-like behavior.

Received Jan. 29, 2021; revised Oct. 11, 2021; accepted Oct. 13, 2021.

Author contributions: L.A.V., R.S.C., D.S.-O., R.S.G., J.M.T., and M.C.B. designed research; L.A.V., D.S.-O., R.S.G., J.M., E.P.A., N.T., and C.D.R. analyzed data; L.A.V. edited the paper; L.A.V. and R.S.C. wrote the paper; R.S.C., G.A.N., D.S.-O., R.S.G., N.R.D., J.M., V.C.D.B., E.P.A., N.F.M., A.M.Z., N.T., C.D.R., J.M.T., and M.C.B. performed research; R.S.C. wrote the first draft of the paper; J.M.T. and M.C.B. contributed unpublished reagents/analytic tools.

This work was supported by Conselho Nacional de Desenvolvimento Cientifico e Tecnológico, INCT-Neuroimmunomodulation, Coordenadoria de Aperfeiçoamento de Pessoal de Nível Superior. R.S.C. was supported by São Paulo Research Foundation FAPESP #2016/00977-2. We thank Erika Roman, Marcio Cruz, and Gerson Ferraz for laboratory management.

The authors declare no competing financial interests.

Correspondence should be addressed to Licio A. Velloso at lavellos@unicamp.br.

https://doi.org/10.1523/JNEUROSCI.0222-21.2021

Introduction

The hypothalamic melanocortin system plays a central role in the regulation of whole-body metabolism by integrating signals involved in the control of food intake, energy expenditure, and nutrient storage and utilization (Kuhnen et al., 2019; da Silva et al., 2020). In both experimental models and humans, genetic defects affecting key components of this system result in the development of obesity (Huszar et al., 1997; Krude et al., 1998; Hinney et al., 1999; Bumaschny et al., 2012). In addition, in experimental diet-induced obesity (DIO), which is used as a model for the more prevalent forms of nonmonogenic human obesity, proopiomelanocortin (POMC) regulation in response to feeding is affected rapidly (Souza et al., 2016); and in the long-run, POMC neurons can undergo apoptosis (Moraes et al., 2009; Yi et al., 2017). Thus, the detailed characterization of components of the hypothalamic melanocortin system undergoing abnormal regulation in obesity could provide advances in the development of strategies to prevent and treat obesity.

Nescient helix-loop-helix 2 (NHLH2) is a basic helix-loop-helix transcription factor that is highly expressed in the mediobasal hypothalamus (Al Rayyan et al., 2014), where it controls the transcription of prohormone convertase 1/3 (*Pcsk1*, PC1/3) and thus the catalytic processing of POMC into its active derivatives (Jing et al., 2004). The whole-body targeted deletion of the *Nhlh2* gene results in hypogonadism and obesity (Good et al., 1997); and at least in part, the obese phenotype is associated with reduced spontaneous physical activity (Good et al., 2008), implying that NHLH2 is involved in the regulation of a wide range of functions and behaviors that impact on whole-body energy metabolism. A nonsynonymous single nucleotide polymorphism of *NHLH2* has been found in 0.1% of people with obesity, suggesting an involvement of this gene in human obesity (Lewis, 1991; Ahituv et al., 2007). Moreover, a recent study has shown that NHLH2 expression is reduced because of Prader–Willi syndrome chromosome 15q microdeletions that affect the *SNORD116* gene (Burnett et al., 2017). Furthermore, in mice, the paternal KO of *Snord116* recapitulates most of the human phenotype of patients with Prader–Willi syndrome, including the reductions of NHLH2 and its transcriptional target, PC1/3 (Burnett et al., 2017). These findings provide strong evidence for the involvement of NHLH2 in the regulation of behavior and body energy homeostasis in humans, as well as in experimental models.

Despite undisputed clinical and experimental evidence suggesting that NHLH2 could be an attractive target to treat obesity, no previous study has evaluated the outcomes of the hypothalamic overexpression of NHLH2 in obesity. Here, we hypothesized that overexpression of NHLH2 in the hypothalamus could protect from obesity; thus, we used a lentivirus to promote NHLH2 overexpression specifically in the arcuate nucleus (ARC) of DIO mice, which resulted in the mitigation of obesity by reducing caloric intake, increasing spontaneous physical activity, and increasing brown adipose tissue (BAT) thermogenesis; these changes were accompanied by reduced obesity-associated anxiety/depression-like behavior.

Materials and Methods

Analysis of single-cell RNA sequencing data: data acquisition and normalization

Campbell et al. (2017) processed and filtered single-cell RNA sequencing (scRNAseq) data that were obtained as a raw digital gene expression (DGE) matrix from the Single-Cell Portal (https://singlecell.broadinstitute.org/single_cell/data/public/SCP97/a-molecular-census-of-arcuate-hypothalamus-and-median-eminence-cell-types?filename=expression.txt.gz). Normalization was performed within Seurat version 3 (Butler et al., 2018) with SCTransform (Hafemeister and Satija, 2019), a negative binomial regression normalization and variance stabilization model for state-of-the-art processing of scRNAseq data, and the top 5000 most variable genes were selected for downstream analyses.

Table 1. Macronutrient composition of the diets

Component	Chow (g)	HFD (g)
Starch	427.5	115.5
Protein (casein 85%)	200	200
Dextrinized corn starch	132	132
Sucrose	100	100
Soybean oil	40	40
Lard	0	312
Fiber (cellulose)	50	50
Mineral mix (AIN-93)	35	35
Vitamin mix (AIN-93)	10	10
L-Cystine	3	3
Choline bitartrate	2.5	2.5
Total	1000	1000

Dimensionality reduction with diffusion-based manifold approximation and projection

Obtaining a low-dimensional visualization of high-dimensional data, such as scRNAseq data, is a challenging task that can be addressed by dimensionality reduction algorithms, which generate low-dimensional embeddings (i.e., two dimensions) that preserve the most important aspects of the original data. For the purpose of dissecting the cellular heterogeneity in the ARC and determining the cellular distribution of *Nhlh2*, we used diffusion-based Manifold Approximation and Projection (dbMAP), a dimensionality reduction method recently developed by our group (http://dx.doi.org/10.2139/ssrn.3582067) and publicly available at https://github.com/davisidarta/dbMAP. Briefly, dbMAP first consists of an adaptive multiscale diffusion maps approach that preserves the intrinsic dimensionality of data while embedding it into a lower dimensional structure before layout. This information is still high-dimensional, and an optimized Uniform Manifold Approximation and Projection (Becht et al., 2018) is then used for a second, sequential approximation of the Laplace–Beltrami operator to generate a low-dimensional visualization. For the analysis shown in this manuscript, the diffusion basis was extracted from the data neighborhood graph by using the top 5000 highly variable genes and each cell's 15 nearest neighbors into 200 latent diffusion components; next, Uniform Manifold Approximation and Projection was performed by using the following parameters for visualization: minimal distance, 0.3; spread, 1.5; and 1000 training epochs.

Visualization of gene expression

Gene expression was visualized with Seurat version 3 functions in R. For visualization within dbMAP embeddings, the FeaturePlot function was used with default parameters. For visualization of coexpression between *Nhlh2* and *Pomc* or *Kiss1*, the blend parameter was toggled. Dotplots were generated with Seurat's DotPlot function with default parameters. For all visualizations, the main cell types and neuronal subclusters previously defined (Campbell et al., 2017) were used, as they were found to correctly represent most of the structure uncovered by dbMAP.

Analysis of Nhlh2 transcriptional network

The *arboreto* (Van de Sande et al., 2020) workflow within the pySCENIC software suite (Aibar et al., 2017) was used to compute the gene regulatory networks (GRNs) of ARC neurons only, after excluding the remaining cell types. The pySCENIC suite identifies and weights regulons (transcriptional factors and their associated target genes) in single-cell data by using *arboreto* to identify coexpression of both transcriptional factors and their targets in the same cell, one cell at a time. The learned GRNs are then weighted against known databases of motifs, enhancers, and promoter regions, thus linking existing genomic knowledge to the exploration of cell-specific transcriptional dynamics. Five distinct

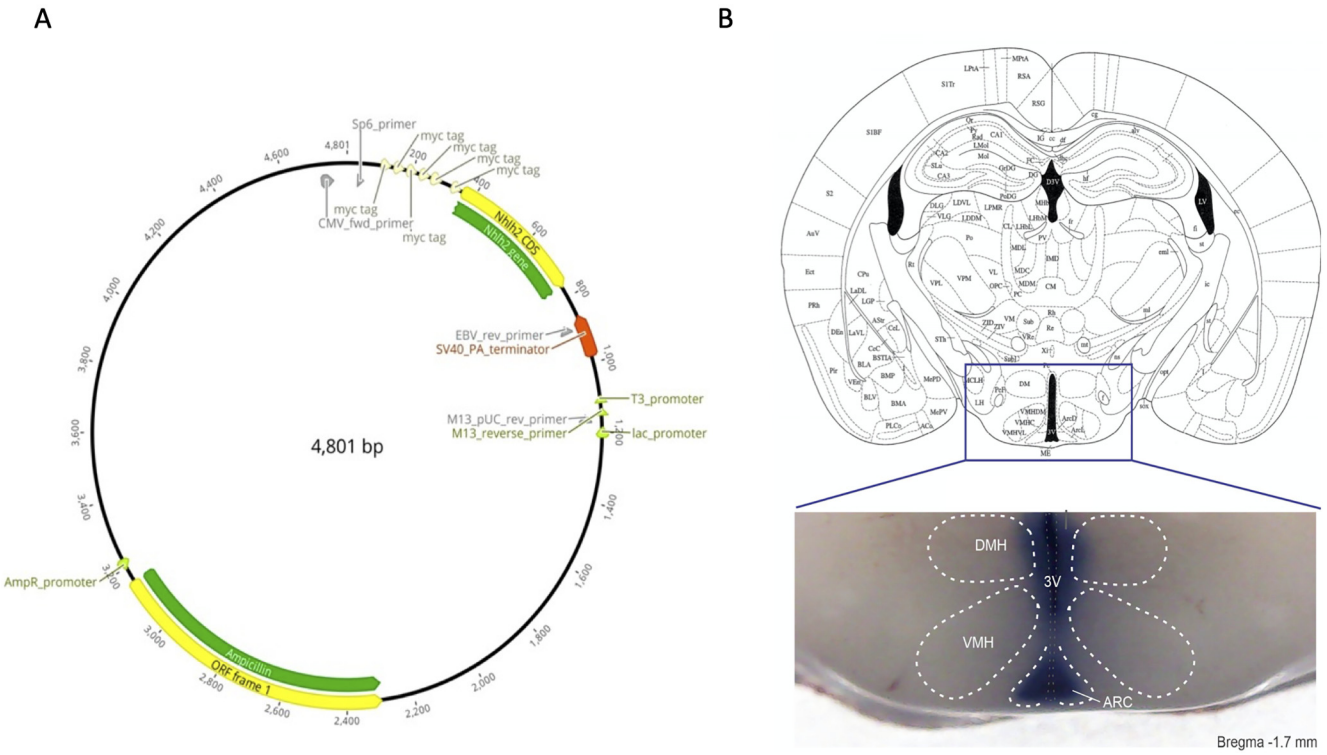

Figure 1. Lentiviral vector and injection site. ***A***, Schematic representation of the overexpression-inducing recombinant lentiviral vector harboring a tissue-specific Nhlh2 expression cassette. ***B***, The accuracy of lentiviruses injections site was determined by injecting Evans blue and dissecting the region of interest for inspection. Image is representative of five independent experiments.

promoter regions were considered around the transcription start site (TSS), as per default: 500 bp upstream of the TSS, 500 bp upstream and 100 bp downstream of the TSS, 5 kb around the TSS and 10 kb around the TSS. Regulons containing at least 10 target genes were kept for downstream analysis. After identification of NHLH2 transcriptional targets, the relative importance for each was retrieved from the adjacency matrix generated with *arboreto* representing NHLH2 GRN, and the top 50 targets with the highest relative importance were used for visualization. To validate whether the genes thereby identified as NHLH2 transcriptional targets by this workflow contained known E-box motifs (CANNTG), we retrieved the sequences from their promotor regions (1000 bp upstream of the TSS) using the University of California–Santa Cruz Genome Browser (Kent et al., 2002) (the *mm9* genome build was used), and generated custom code with the R programming language to survey their sequences for all possible motifs. We found that only 8 genes of the 116 predicted targets did not contain these motifs in their promoter regions 1000 bp upstream of the TSS (a narrower region than the surveyed by *arboreto*): *Tmem35*, *Nkx2.1*, *HQ.Q2*, *Fam159a*, *Tmem8c*, *Lrrc38*, *Gnai1*, and *X4932443I19Rik* (a proposed, theoretical gene). The adopted strategy holds two limitations: its reliance on known motifs by *arboreto* and the choice of 1000 bp upstream of the TSS cutoff for validation. Thus, it is possible that these 8 genes also hold E-box motifs in their promoter regions, albeit at greater distances from the TSS. Nevertheless, this approach resulted in a 93.1% (108 of 116) accuracy score when predicting NHLH2 transcriptional targets, which so far have remained unknown.

Analysis of NHLH2 transcriptional targets in the BXD mouse families

The BXD is a mouse reference population composed of recombinant inbred cohorts generated from the crossing of C57BL/6J (B) and DBA/2J (D), originating lineages that are diverse in their gene expression patterns and phenotypes (Andreux et al., 2012). Based on GRN analysis of arcuate neurons, the top transcriptional targets correlated with NHLH2 in the hypothalamus (INIA Hypothalamus Affy MoGene 1.0 ST [Nov10]) of BXD mice families (Andreux et al., 2012) were analyzed. Heatmap visualization was performed using Gene-E. Expression values across different mice families were sorted based on *Nhlh2* levels, and its targets were hierarchically clustered. The data are available at the GeneNetwork (http://www.genenetwork.org).

Experimental animals

Male and female Swiss mice were used in this study. Mice were bred at the animal facility of the University of Campinas and maintained in individual cages in a 12 h photoperiod at 22°C-24°C with *ad libitum* food and water. The number of mice in each experiment is presented in the figure legends. All experimental procedures were approved by the Animal Research Ethics Committee of the University of Campinas (#4072-1).

Dietary interventions and experimental approach

For the experiment depicted in Figure 6*A*, 8-week-old mice were weighed, numbered, and submitted to body mass *z*-score separation into 11 groups. One group was fed chow and was regarded as the baseline control. The remaining 10 groups were fed a high-fat diet (HFD, composition in Table 1) for 3, 6, or 12 h; 1, 3, 5, or 7 d; or yet 2, 4, or 8 weeks. At the end of the experimental period, mice were submitted to lethal anesthesia and the hypothalamus was extracted for analyses. The experiment was performed on reverse timing; thus, at the end of the experimental time, all mice were at the same age. For the experiment depicted in Figure 6*B*, 8-week-old male mice fed on chow were divided randomly into two groups: one group was fasted for 12 h and the other group was fasted for 10 h; and then chow was reintroduced for refeeding for 2 h. At the end of the experimental time, mice were submitted to lethal anesthesia and the hypothalamus was extracted for analyses. For the experiment depicted in Figure 6*C*, 8-week-old male mice fed on chow were divided randomly into three groups: one group was fasted for 12 h, one group was fasted for 12 h and submitted to the intraperitoneal injection of 100 µl of saline, and one group was fasted for 12 h and submitted to the intraperitoneal injection of 100 µl of leptin (10^{-4} M). After 2 h, mice were submitted to lethal anesthesia and the hypothalamus was extracted for analyses. For the remaining of the experiments depicted in Figure 6 and experiments depicted in Figures 7-10, Tables 4 and 5, and Extended Data Figs 7-1 and 9-1, the protocols are depicted in Figure 6*E*;

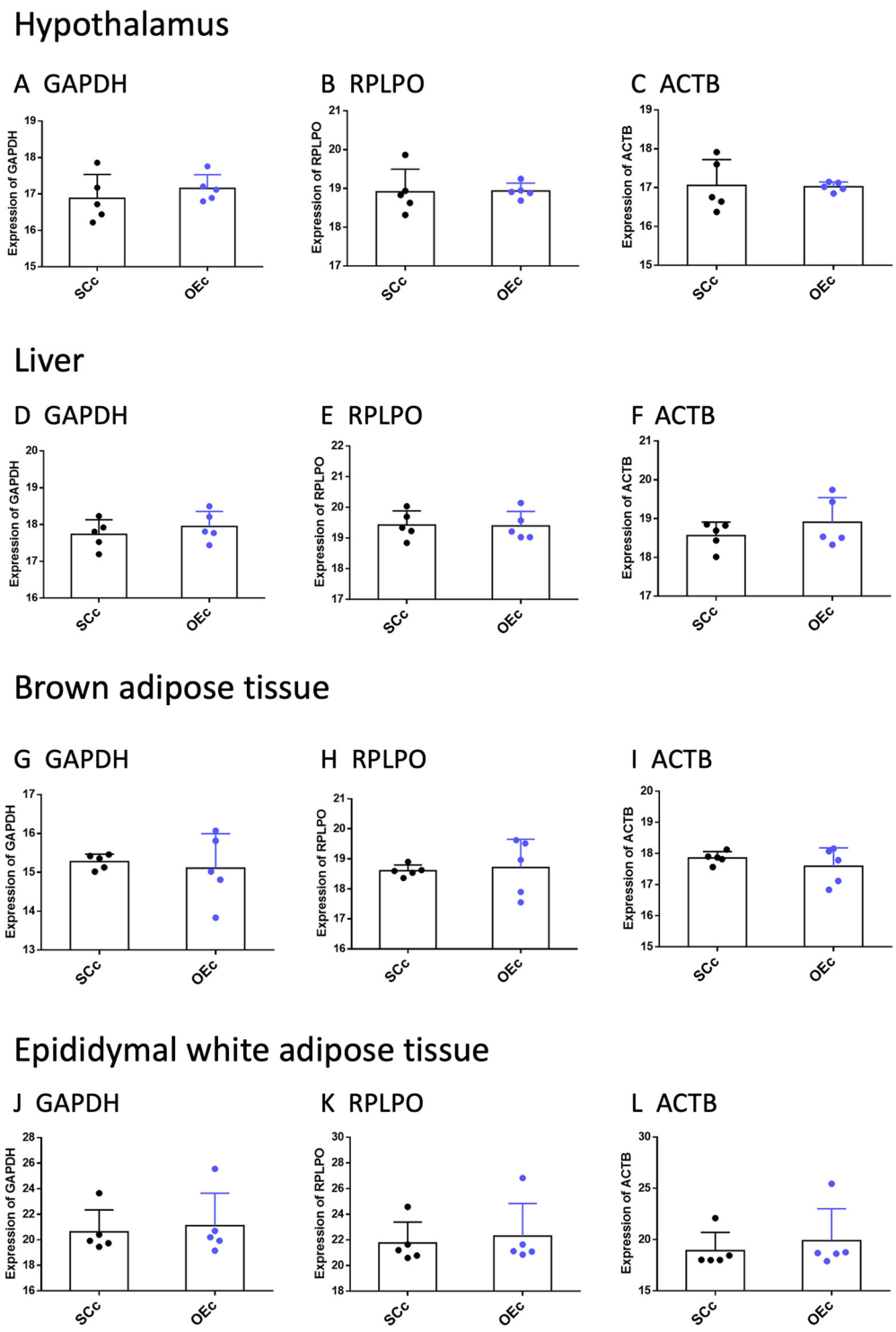

Figure 2. Testing expression stability of housekeeping genes. Real-time PCR determination of the expression of housekeeping genes, *Gapdh*, *Rplpo*, and *Actb*, in the hypothalamus (***A-C***), liver (***D-F***), BAT (***G-I***), and epididymal white adipose tissue (***J-L***). In all experiments, $n = 5$. SCc, Scrambled fed on chow; OEc, overexpression fed on chow.

for the experiments depicted in Figures 11-13, the protocols are depicted in Figure 11*A*.

Site-specific lentiviral inhibition and overexpression of NHLH2 in the ARC

For the lentiviral modulation of NHLH2 in the ARC, 8-week-old mice were anesthetized with a solution of ketamine, xylazine, and diazepam (100, 10, and 5 mg/kg, respectively) and placed in a stereotactic apparatus. Using a Hamilton syringe, lentiviruses (1 µl) were injected bilaterally into the ARC according to the following stereotaxic coordinates: anteroposterior −1.7 mm; lateral ± 0.3 mm; and dorsoventral −5.3 mm. Thereafter, mice were maintained in isolated cages for further experimental analyses. For NHLH2 inhibition, we used a commercially available lentivirus (TRCN 0000084661 from Sigma-Aldrich), whereas for overexpression, we used a recombinant lentiviral vector harboring a tissue-specific *Nhlh2* expression cassette. The plasmid encoding the lentiviral vector backbone was originally produced at the Laboratory of Thomas Braun and Max Planck and kindly donated by Deborah J. Good (Virginia Tech) (Fox and Good, 2008; Wankhade and Good, 2011; Al Rayyan et al., 2013). The lentivirus particles (Fig. 1*A*) were generated by

the Viral Vector Laboratory at the Brazilian Biosciences National Laboratory at the National Center for Research in Energy and Materials, as previously described (Strauss et al., 2006). The gene sequence was identical to Swiss mice *Nhlh2* as determined using the JAX-MGI engine (http://www.informatics.jax.org). The efficiency of the lentivirus was determined in pilot experiments using an anti-flag (myc) antibody and proven efficient to increase NHLH2 expression by 50%. The efficiency of the lentiviruses was assessed by infecting Neuro 2a and CLU189 cells with 10^6 viral particles and determining NHLH2 expression in cell extracts by means of real-time PCR. The accuracy of the injection site was evaluated by the injection of Evans blue (Fig. 1*B*) and determination of the target transcripts by means of real-time PCR. Control mice were always injected with vectors with scrambled sequences.

Dissection of the hypothalamus

For immunoblot and real-time PCR experiments, hypothalami were dissected according to the following coordinates: anterior, optic chiasm; posterior, mammillary bodies; lateral, optic tracts; superior, apex of the hypothalamic third ventricle.

Immunoblots

Tissue samples were homogenized in ~10 volumes of solubilization buffer containing 1% Triton X-100, 100 mM Tris, pH 7.4, 100 mM sodium pyrophosphate, 100 mM sodium fluoride, 10 mM EDTA, 10 mM sodium vanadate, 2 mM PMSF, and 0.1 mg/ml of aprotinin at 4°C. The homogenates were centrifuged at 11,000 rpm at 4°C for 40 min to remove insoluble material. The total protein concentration of the supernatant was determined using the biuret method and reading at 540 nm. Samples of the supernatants containing 50 µg of total protein were resuspended in Laemmli buffer and applied onto polyacrylamide gel for electrophoretic separation (nondenaturing gel). The separated proteins were transferred to a nitrocellulose membrane. Antibody binding to nonspecific proteins was minimized by pre-incubation of the nitrocellulose membranes with blocking buffer (5% nonfat milk powder, 10 mM Tris, 150 mM NaCl, and 0.02% Tween 20) for 1 h. Then, the nitrocellulose membranes were incubated with a specific antibody against NHLH2 (H00004808-M02, Thermo Fisher Scientific). The antigen-antibody complex attached to the nitrocellulose membrane was detected by chemiluminescence using an GE Healthcarekit and following the manufacturer's guidelines. The homogeneity of loading was determined by reblotting the membranes with an anti-α-tubulin antibody (ab7291, Abcam). The identified bands were quantified by means of optical densitometry.

RNA extraction and real-time PCR

Tissue samples were homogenized in TRIzol reagent (Invitrogen) and then centrifuged at 10,500 rpm for total RNA isolation. RNA integrity was determined in agarose gel electrophoresis. Aliquots of 3.0 µg of RNA were submitted to reverse transcription using the High-Capacity cDNA Reverse Transcription Kit (Applied Biosystems). Real-time PCRs were performed by using the TaqMan system (Applied Biosystems). The *Gapdh* gene was chosen as an endogenous reaction control; it served to normalize the expression of the genes of interest in the different samples; *Gapdh* gene expression stability under experimental conditions was tested in all tissues evaluated in this study and was compared with the expression of two other housekeeping genes, *Rplpo* and *Actb* (Fig. 2*A–L*). Before starting the experiments, the system was validated to evaluate whether the amplification efficiencies were similar and close to 100%. The validation consisted of amplifying the cDNAs in triplicate at seven different concentrations (threefold serial dilutions) of a sample chosen at random, both with the oligonucleotides of the gene of interest and of the endogenous control. Then, a standard curve was constructed from the logarithm of the concentration of the samples by threshold cycle, or the cycle in which each amplification curve crosses the detection threshold, which was defined arbitrarily. In this curve, the values of the slope of the curve and the reliability of the replicates were obtained. Thus, the efficiency of the system was calculated using the formula: $E = 10^{(-1/\text{slope})} - 1$. For the relative quantification of the gene under study, real-time PCRs were performed in triplicate using 3.0 µl of TaqMan Universal PCR Master Mix 2×, 0.25 µl of oligonucleotide solution and probe, 0.25 µl of water, and 4.0 µl cDNA (40 ng). The negative control was performed with 4.0 µl of water, instead of cDNA. The cycles used in the thermal cycler were 95°C for 2 min, followed by 40 cycles of 95°C for 5 s and 60°C for 30 s. The relative gene expression values were obtained by analyzing the results in the StepOne Plus System Software program (Applied Biosystems). All primers used in this study are listed in Table 2.

Table 2. Primers used in real-time PCR determinations[a]

Gene name	Assay	Ref Seq
Actb	Mm04394036_g1	AK_075973.1
Cartpt	Mm04210469_m1	NM_001081493.2
F4/80	Mm00802529_m1	NM_010130.4
Gapdh	Mm99999915_g1	NM_001289726.1
Il1β	Mm00434228_m1	NM_008361.3
Mcp-1	Mm03058063_m1	NM_008553.4
Nhlh2	Mm01305580_m1	NM_178777.3
PC1/3	Mm00479023_m1	NM_013628.2
Pomc	Mm00435874_m1	NM_001278581.1
Rplp0	MmPT584394205	NM_007475.1
Tnf	Mm00443258_m1	NM_001278601.1

[a]All primers were purchased from Applied Biosystems.

Indirect calorimetry and locomotor activity

Oxygen consumption ([dot]VO_2), carbon dioxide production ([dot]VCO_2), energy expenditure, and total locomotor activity were measured by using an indirect open-circuit calorimeter (LE405 gas analyzer, Panlab/Harvard Apparatus). Mice were allowed to adapt for 12 h before data were recorded for 24 h (light and dark cycles).

Thermographic determinations

For determination of interscapular BAT, an infrared camera was used with an infrared resolution of 320 × 240 pixels and a thermal sensitivity and NETD of b40mKat at 30°C (FLIR T450sc, FLIR Systems). Images are presented in the rainbow high-contrast mode that is available in the color palette of the FLIR Tools software.

Determination of lean and fat mass

Mice were anesthetized, and the body fat mass and lean mass contents were measured with a DXA system, according to the manufacturer's recommendations (Discovery Wi QDR Series; Hologic Apex Software, Hologic).

Adipocyte area

The area of the adipocytes was determined by using paraffinized sections of adipose tissue examined with ImageJ software. Adipocytes were then counted, and the absolute pixel area of each cell was calculated and converted to μm^2.

H&E staining

The tissue was stored in 4% PFA for 24 h, then placed in 70% alcohol, and then embedded in paraffin and sectioned.

Behavioral tests

All tests were performed during the light period of the cycle, in an environment with complete silence and illumination sufficient for recording (60 lux). Test sequence was random, and there were 3 d resting intervals between tests. Mice were habituated previously to the environments for 24 h and submitted to minimal human handling during the tests. All arenas were properly cleaned after each determination. For elevated plus maze and open field tests, scores were obtained from the equipment's software. For tail suspension, rotarod, and treadmill tests, scores were provided by the mean scores given by 3 individual observers; 2 observers were blind to the experimental conditions.

Elevated plus maze test. Open arms were 6 × 35 cm and closed arms were 6 × 35 × 20 cm; the central arena was 6 × 6 cm; the high from the floor was 75 cm. There were three sensors in each arm. Mice were placed in the central arena of the maze with their head facing the closed space.

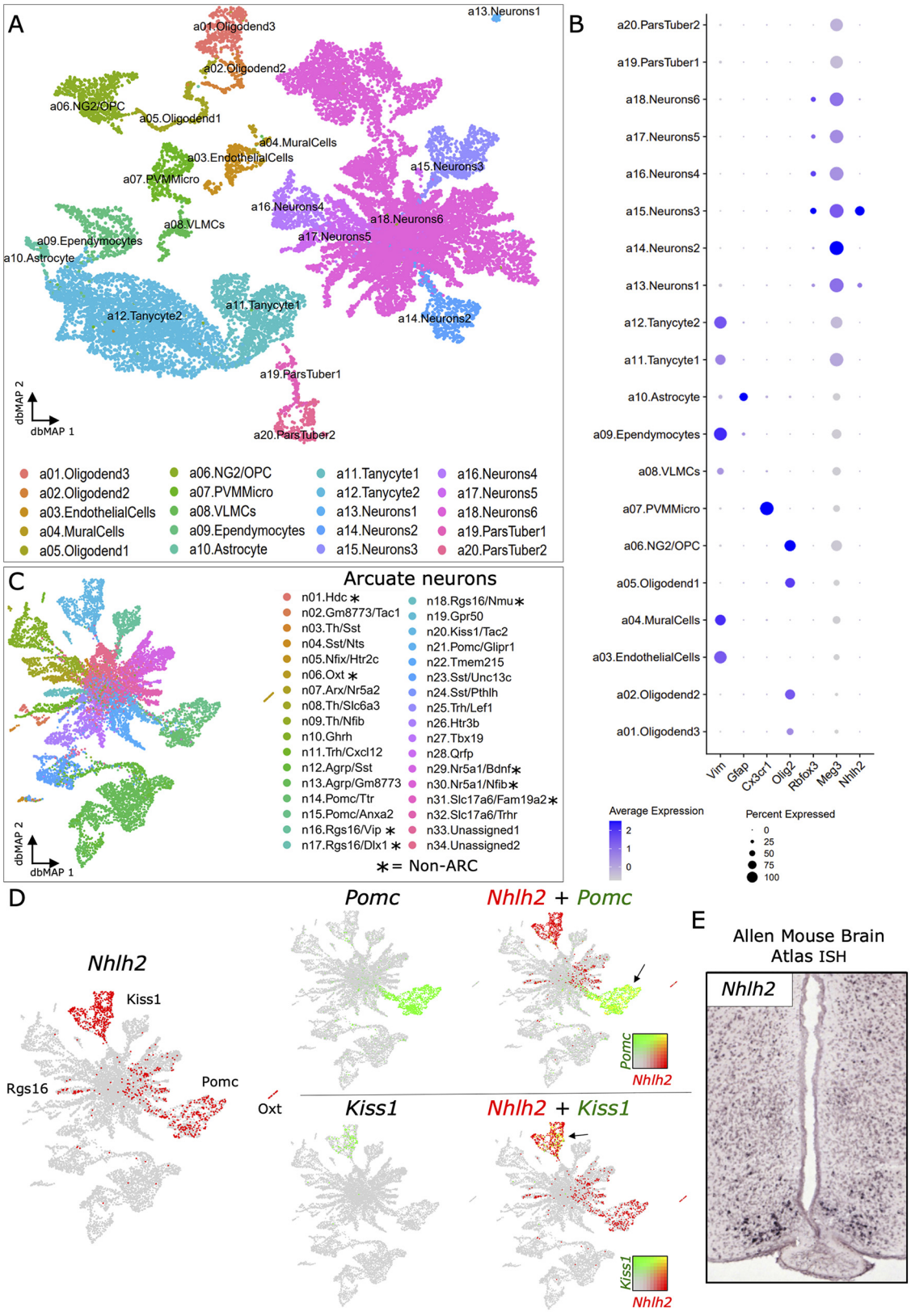

Figure 3. Analysis of ARC scRNAseq data. ***A***, dbMAP representation of 20,921 cells from the ARC and median eminence (ME) of adult mice (DOI: 10.1038/nn.4495). Each dot represents a single-cell transcriptome. Its distance from other cells represents phenotypic (transcriptional) similarity. Cells are colored by the main cell types defined in the adult ARC-ME (DOI: 10.1038/nn.4495). ***B***, Dot plot visualization of *Nhlh2* and main cell type markers (*Vim*, tanycytes; *Gfap*, astrocytes; *Cx3cr1*, microglia; and *Rbfox3* and *Meg3*, neurons). As shown, *Nhlh2* is selectively expressed by neuronal populations. ***C***, dbMAP representation of ARC neurons. Cells are colored by neuronal subclusters previously defined, and non-ARC subpopulations are marked (*). ***D***, Visualization of *Nhlh2* expression in the dbMAP neuronal embedding. *Nhlh2* is expressed by POMC, KISS1, OXT, and Rgs16 neurons (left). Markers of these neuronal subpopulations, such as *Pomc* and *Kiss1*, are consistently coexpressed with *Nhlh2* (right). ***E***, Visualization of *Nhlh2* expression in the ARC by ISH of a coronal slice in a 56-d-old mouse brain, retrieved from the Allen Mouse Brain Atlas (https://mouse.brain-map.org/experiment/show/74657929).

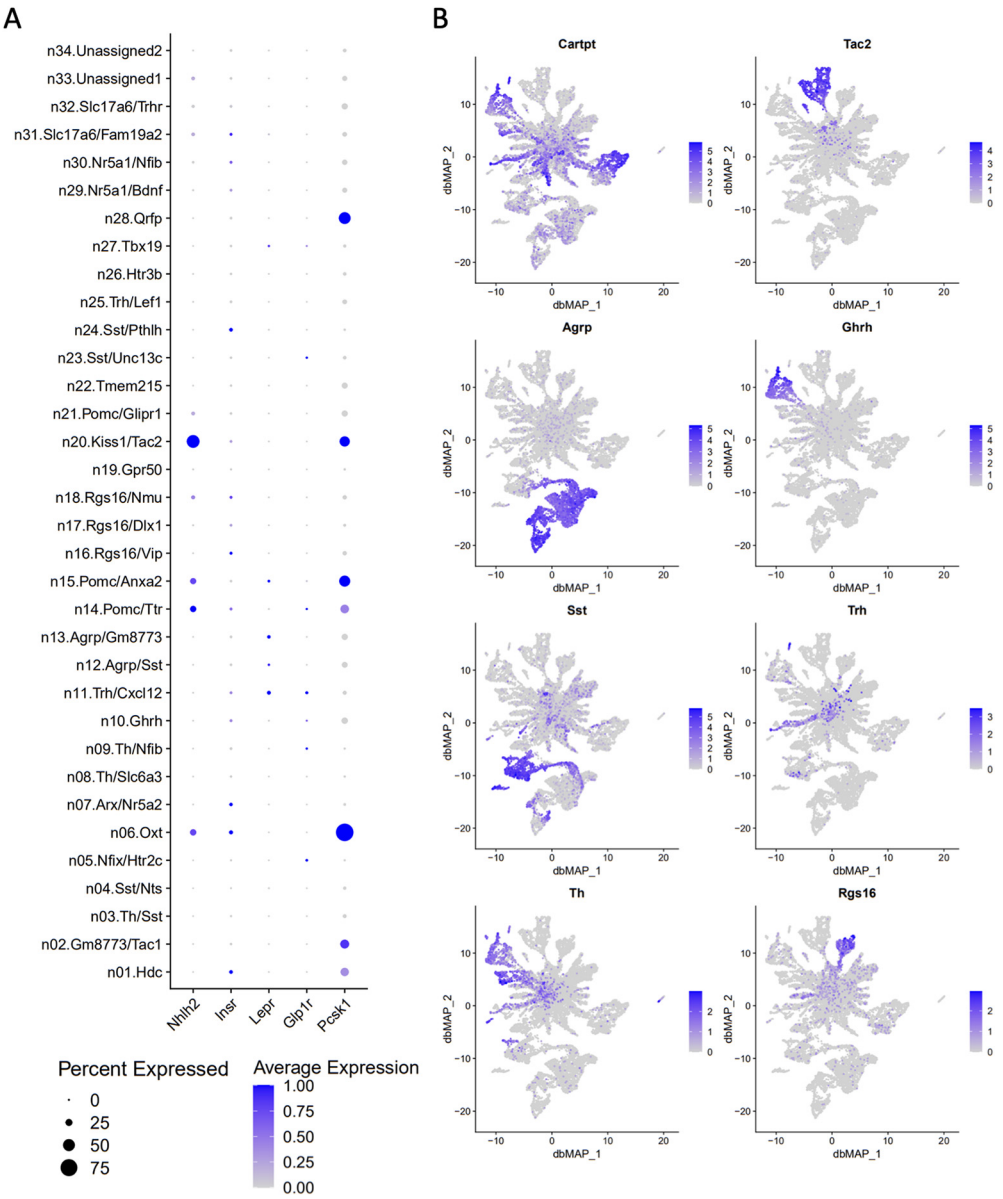

Figure 4. Visualization of gene expression in ARC neurons. ***A***, Dot plot visualization of *Nhlh2*, *Insr*, *Lepr*, *Glp1r*, and *Pcsk1* expression in the ARC-ME scRNAseq neuronal clusters. ***B***, Panel of gene expression visualization in the neuronal dbMAP embedding, showing major subpopulation markers.

Recording took place for 5 min. The results are expressed as percent time spent in open and closed arms (Pellow et al., 1985).

Open field test. The test was performed by using activity boxes (INSIGHT) equipped with 6 bars with 16 sensors that continuously detected and monitored the position of mice; the field was 50 × 50 cm. Mice were placed in the center of the field, and determinations took place for 5 min. During the experiments, the positions of mice were registered continuously and stored, allowing a detailed analysis of distance covered, average speed, time immobile, ambulatory movements, and time spent in the center. For time spent in the center, the results are expressed as the percentage of total time; for ambulatory activity, the results are expressed in meters.

Tail suspension test. The procedure consisted of suspending each mouse by the tail, with the aid of an adhesive tape at a height of 1.5 m from the floor, so that mice remained with the ventral portion of the body facing the observer. Each experimental animal remained in this position for 6 min; and the latency to immobility as well as the total immobilized time were measured throughout the experiment. The results are expressed in seconds.

Rotarod test. Mice were trained on the cylinder while maintaining a constant rotation of 20 rpm for a maximum of 2 min; training occurred 24 h before the test and consisted of four 2 min trials, separated by 15 min resting intervals. During the test, mice were placed on the equipment cylinder and submitted to an automatic acceleration protocol increasing from 5 to 42 rpm over a period of 6 min (acceleration of 6.2 rpm/minute). Each test session consisted of three trials, separated by 15 min resting intervals. The results are expressed as the mean time to fall (minutes) and the mean acceleration when a fall occurred (rpm); the fall height was 20 cm.

Treadmill test. In all experiments, we used a treadmill with individual tracks designed for small animals, without electrical stimulation, and with an inclination of 10°. Two days before the test, the mice underwent a treadmill adaptation protocol. On the first day, mice were submitted to a 20 min run at 10 cm/s. On the second day, the mice were submitted to a 5 min run at 10 cm/s, followed by an acceleration of 0.1 cm/s until reaching the speed of 40 cm/s, which was maintained for 15 min. On the third day, when the test was performed, the mice were placed on the treadmill with an initial speed of 10 cm/s and acceleration of 0.1 cm/s until reaching a speed of 40 cm/s. Then, mice remained on the test for an additional 55 min, totaling 60 min of test.

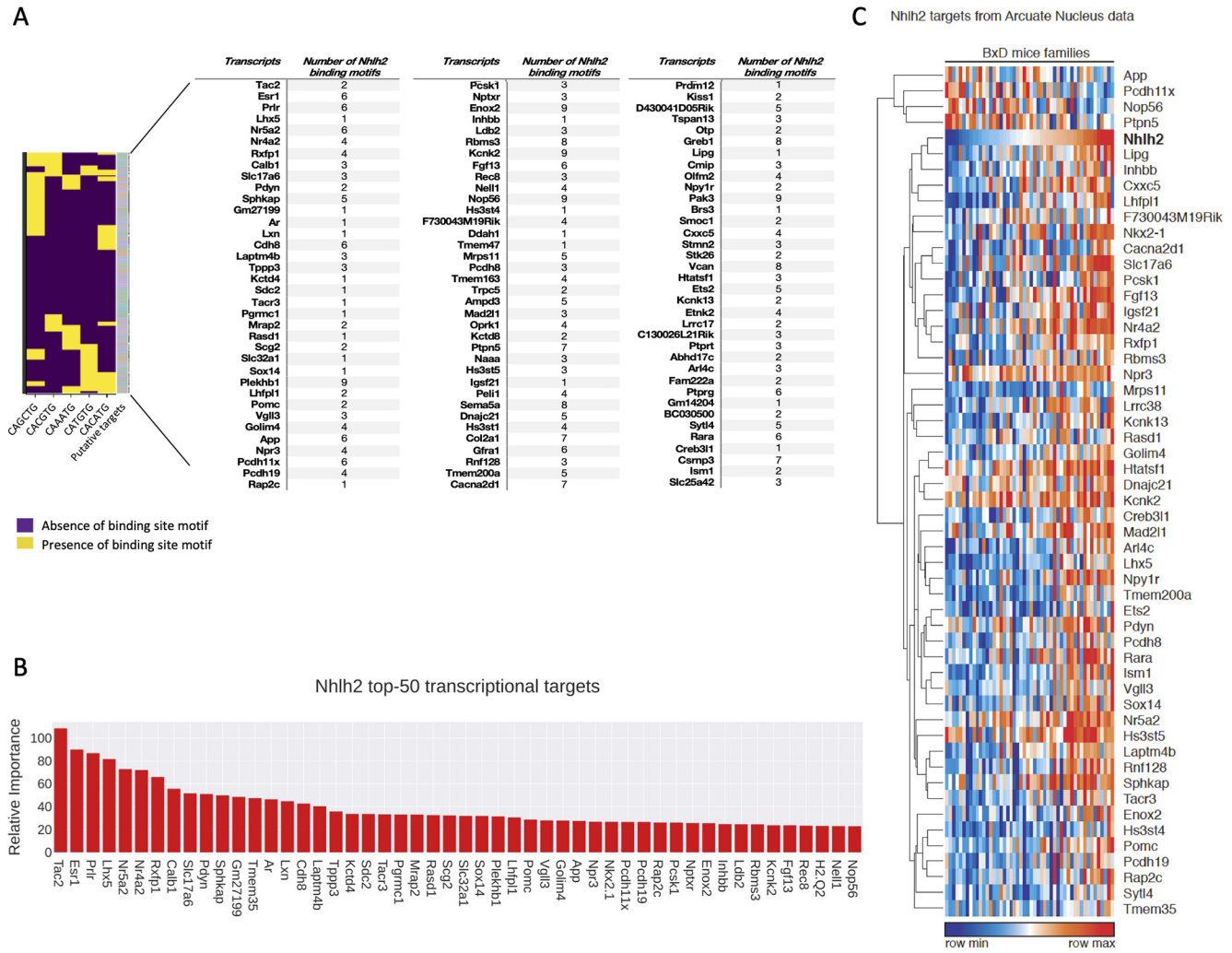

Figure 5. NHLH2 transcriptional targets. ***A***, The heatmap in the left-hand part of the figure represents the presence or absence of binding site motifs for NHLH2 in putative gene targets. Genes and number of NHLH2 binding motifs are depicted in the tables. One gene target may present more than one of each of the binding motifs; hence, the number of NHLH2 binding motifs may be >5. ***B***, Graphic representation of the 50 major NHLH2 transcriptional targets determined using the GRNs. ***C***, NHLH2 hypothalamic targets identified in the BXD mice families.

Sexual behavior and gonad morphology

Determination of sexual behavior was performed as described previously (Ahlenius and Larsson, 1984). Briefly, 10-week-old female mice were submitted to estrus determination by vaginal cytology. Once estrus was confirmed, female mice were allocated to a cage (Universal Mouse Innocage, 522.6 cm^2 floor space, 5653.5 cm^3 living space, 12.7 cm height) alongside one 10-week-old male. Recording was performed with a Canon camera model EOS Rebel T5i for 30 min. The following parameters were determined: mount frequency, intromission frequency, ejaculation frequency, latency for the first mount, latency for first intromission, latency for first ejaculation, total mounts, and total mount attempts. A sexual behavior index was obtained by the sum of events of all parameters evaluated and used for comparison among groups. Two days after sexual behavior evaluation, gonads were extracted for measurement and histologic evaluation.

Statistical analysis

The results are presented as means and SDs of the means. For each experiment, the sample size was defined in advance by power analysis (Festing and Altman, 2002). For statistical analysis, Levene's test was applied to determine the homogeneities of the variances, and the Kolmogorov–Smirnov test was used to determine normality of the distribution. For comparison of two groups, Student's *t* test was used for parametric data, and Kruskal–Wallis was used for nonparametric data. For comparison of three or more groups, ANOVA was used; and when indicated, the Tukey's honestly significant difference test was used for multiple comparisons of means. In all cases, the level of significance for rejection of the null hypothesis was 5% ($p < 0.05$). The data were analyzed by using the software Statistic for Windows, version 7.0 (StatSoft). Open-source code in the R programming language for reproducing this analysis is available at https://github.com/OCRC/Carraro-et-al_2021.

Results

Nhlh2 is expressed in POMC and Kiss1 neurons in the adult murine ARC

Previously, the cellular distribution of NHLH2 in the hypothalamus was determined by means of histology-based methods (Cogliati et al., 2007; Schmid et al., 2007; Vella et al., 2007). Here, we evaluated single-cell transcriptomes to refine the characterization of ARC cell subpopulations expressing *Nhlh2*. Initially, we performed a general assessment of *Nhlh2* expression in adult mice analyzing 20,921 previously sequenced single-cell transcriptomes from the ARC and the median eminence (Campbell et al., 2017) (Fig. 3*A*). This analysis revealed that *Nhlh2* expression was restricted to the neuronal populations (Fig. 3*B*) and predominantly KISS1 and POMC neurons (Fig. 3*C*,*D*). Spatially, *Nhlh2* expression in the hypothalamus is mostly confined to the ARC, although other nuclei also present a few *Nhlh2*-expressing cells

Table 3. Functions and medical conditions associated with the main putative targets of NHLH2

NHLH2 targets	Gene product function	Diseases and medical conditions
Lhx5	Regulation of neuronal differentiation and migration	Scapuloperoneal spinal muscular atrophy and scapuloperoneal myopathy
Nr5a2	Nuclear receptor that acts as a key metabolic sensor by regulating the expression of genes involved in bile acid synthesis, cholesterol homeostasis, and triglyceride synthesis	Hepatitis B, maturity-onset diabetes of the young, and cholestasis and benign recurrent intrahepatic
Nr4a2	Transcriptional regulator which is important for the differentiation and maintenance of meso-diencephalic dopaminergic (mdDA) neurons during development	Parkinson's disease, late-onset and arthritis
Rxfp1	The activity of this receptor is mediated by G proteins leading to stimulation of adenylate cyclase and an increase of cAMP	Placenta accreta and endometriosis
Slc17a6	Mediates the uptake of glutamate into synaptic vesicles at presynaptic nerve terminals of excitatory neural cells	Amelogenesis imperfecta and arthrogryposis
Pdyn	Plays a role in a number of physiologic functions, including pain perception and responses to stress	Spinocerebellar ataxia 23 and drug dependence
Sphkap	Acts as a converging factor linking cAMP and sphingosine signaling pathways; plays a regulatory role in the modulation of SPHK1	Renal cell carcinoma and papillary
Tmem35	A soluble peptide released by shedding may interact with NGFR and modulate neurite outgrowth	Schizophrenia and Alzheimer's disease
Laptm4b	Blocks EGF-stimulated EGFR intraluminal sorting and degradation; plays a role as negative regulator of TGFB1 production in regulatory T cells; binds ceramide and facilitates its exit from late endosome in order to control cell death pathways	Mucolipidosis and gallbladder sarcoma
Tacr3	Receptor for the tachykinin neuropeptide neuromedin-K; associated with G proteins that activate a phosphatidylinositol-calcium second messenger system	Hypogonadotropic hypogonadism 11 with or without anosmia and normosmic congenital hypogonadotropic hypogonadism
Rasd1	Negatively regulates the transcription regulation activity of the APBB1/FE65-APP complex via its interaction with APBB1/FE65	Malt Worker's lung and prostate leiomyosarcoma
Sox14	Acts as a negative regulator of transcription; SRY-related HMG box gene 14, predominantly expressed in fetal brain, spinal cord, thymus, potentially involved in regulation of nervous system development, modulator of LINE retroposon promoter activity SOX14	Blepharophimosis and moebius syndrome
Lhfpl1	Lipoma HMGIC (high mobility Group I C protein) fusion partner like gene 1	Branchiootic syndrome
Pcsk1	Involved in the processing of hormone and other protein precursors at sites comprised of pairs of basic amino acid residues; substrates include POMC, renin, enkephalin, dynorphin, somatostatin, insulin, and AGRP	Proprotein convertase 1/3 deficiency and body mass index quantitative trait locus 12
Pomc	Stimulates the adrenal glands to release cortisol; anorexigenic peptide; increases the pigmentation of skin by increasing melanin production in melanocytes; increases the pigmentation of skin by increasing melanin production in melanocytes; endogenous orexigenic opiate	Obesity, early-onset, with adrenal insufficiency and red hair and body mass index quantitative trait locus 11
Vgll3	May act as a specific coactivator for the mammalian TEFs	Juxtacortical osteosarcoma and malignant inflammatory fibrous histiocytoma
Golim4	Plays a role in endosome to Golgi protein trafficking; mediates protein transport along the late endosome-bypass pathway from the early endosome to the Golgi	Spinal muscular atrophy, distal, autosomal recessive and immunodeficiency
App	Increased levels during neuronal differentiation	Cerebral amyloid angiopathy, app-related, and Alzheimer's disease
Npr3	May function as a clearance receptor for NPPA, NPPB, and NPPC, regulating their local concentrations and effects; regulates diuresis, blood pressure, and skeletal development	Functional diarrhea and hypertension
Pcdh11x	Potential calcium-dependent cell-adhesion protein	Dyslexia and schizoaffective disorder
Pcdh19	Potential calcium-dependent cell-adhesion protein	Epileptic encephalopathy, early infantile and childhood absence epilepsy
Rap2c	Plays a role in cytoskeletal rearrangements and regulates cell spreading through activation of the effector TNIK; may play a role in SRE-mediated gene transcription	Pathologic nystagmus
Enox2	May be involved in cell growth	Suppressor of tumorigenicity 3 and variegate porphyria
Inhbb	Inhibins and activins inhibit and activate, respectively, the secretion of follitropin by the pituitary gland; inhibins appear to oppose the functions of activins	Eclampsia and pre-eclampsia
Rbms3	Binds poly(A) and poly(U) oligoribonucleotides	Mental retardation with language impairment and with or without autistic features and Heimler syndrome 2
Kcnk2	Reversibly converts between a voltage-insensitive potassium leak channel and a voltage-dependent outward rectifying potassium channel in a phosphorylation-dependent manner	Posterolateral myocardial infarction and dentin sensitivity
Fgf13	Plays a crucial role in neuron polarization and migration in the cerebral cortex and the hippocampus; required for the development of axonal initial segment-targeting inhibitory GABAergic synapses made by chandelier neurons	Borjeson-Forssman-Lehmann syndrome and X-linked congenital generalized hypertrichosis

(Fig. 3*E*). Next, we demonstrated that populations expressing *Nhlh2* also express *Pcsk1* (gene encoding for PC1/3), as well as transcripts encoding for leptin (*Lepr*) and insulin (*Insr*) receptors (Fig. 4*A*), reinforcing the central role of NHLH2 in energy homeostasis. We further explored the expression of neuronal marker genes in the ARC and showed that transcripts encoding *Cart* and *Tac2* are highly coexpressed with *Nhlh2* (Fig. 4*B*). To identify transcriptional targets for NHLH2, we excluded non-neuronal cells and estimated the GRNs of arcuate neuronal subpopulations and their associated regulons (transcriptional factors and

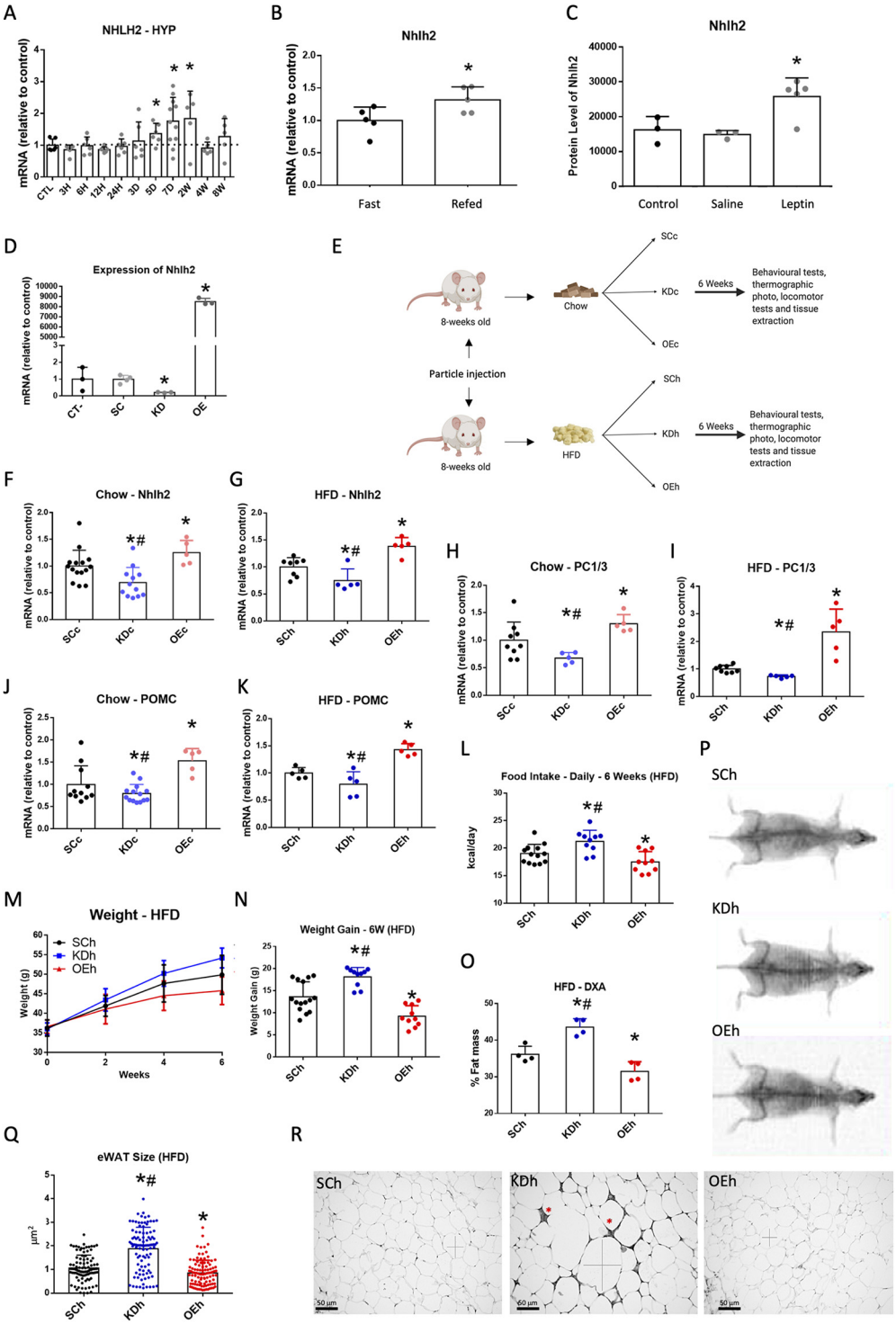

Figure 6. Hypothalamic overexpression of NHLH2 prevents the development of experimental obesity. ***A***, Transcript expression of *Nhlh2* in the hypothalamus of mice fed an HFD for different periods of time. ***B***, Transcript expression of *Nhlh2* in the hypothalamus of fasting and refed mice. ***C***, Protein levels of hypothalamic NHLH2 in mice acutely treated with leptin. ***D***, Transcript expression of *Nhlh2* obtained during the efficiency test of the lentiviruses infecting CLU189 cells with 10^6 viral particles. ***E***, Schematic representation of the protocols used for evaluation of the impact of modulating hypothalamic NHLH2 in mice submitted simultaneously to an HFD and lentivirus injections, the obesity prevention model. The transcript expressions of *Nhlh2* (***F***,***G***), *Pcsk1* (gene coding for PC1/3) (***H***,***I***), and *Pomc* (***J***,***K***) were determined in the hypothalamus of mice submitted to the protocol depicted in ***E***. Mean daily food intake (***L***), body mass (***M***), weight gain (***N***), body adiposity (***O***,***P***), and epididymal white adipose tissue mean adipocyte size (***Q***,***R***) were determined in mice submitted to the protocol depicted in ***E***. ***A***, ***C***, ***D***, $^*p < 0.05$ versus control (CTL). ***B***, $^*p < 0.05$ versus fast. ***F-O***, ***Q***, $^*p < 0.05$ versus scrambled (SCc, scrambled fed chow; SCh, scrambled fed an HFD). $^\#p < 0.05$ versus overexpression (OEc, overexpression fed chow; OEh, overexpression fed an HFD). ***R***, Red asterisk represents crown-like structures. Crossed lines indicate measurement of adipocyte areas. CT, Control; DXA, dual X-ray absorptiometry; eWAT, epididymal white adipose tissue; HYP, hypothalamus; KD, knockdown; KDc, knockdown fed chow; KDh, knockdown fed an HFD; OE, overexpression; OEc, overexpression fed chow; OEh, overexpression fed an HFD; SC, scrambled; SCc, scrambled fed chow; SCh, scrambled fed an HFD. ***A***, ***F-N***, $n = 5$-15; ***B-D***, ***O-R***, $n = 5$.

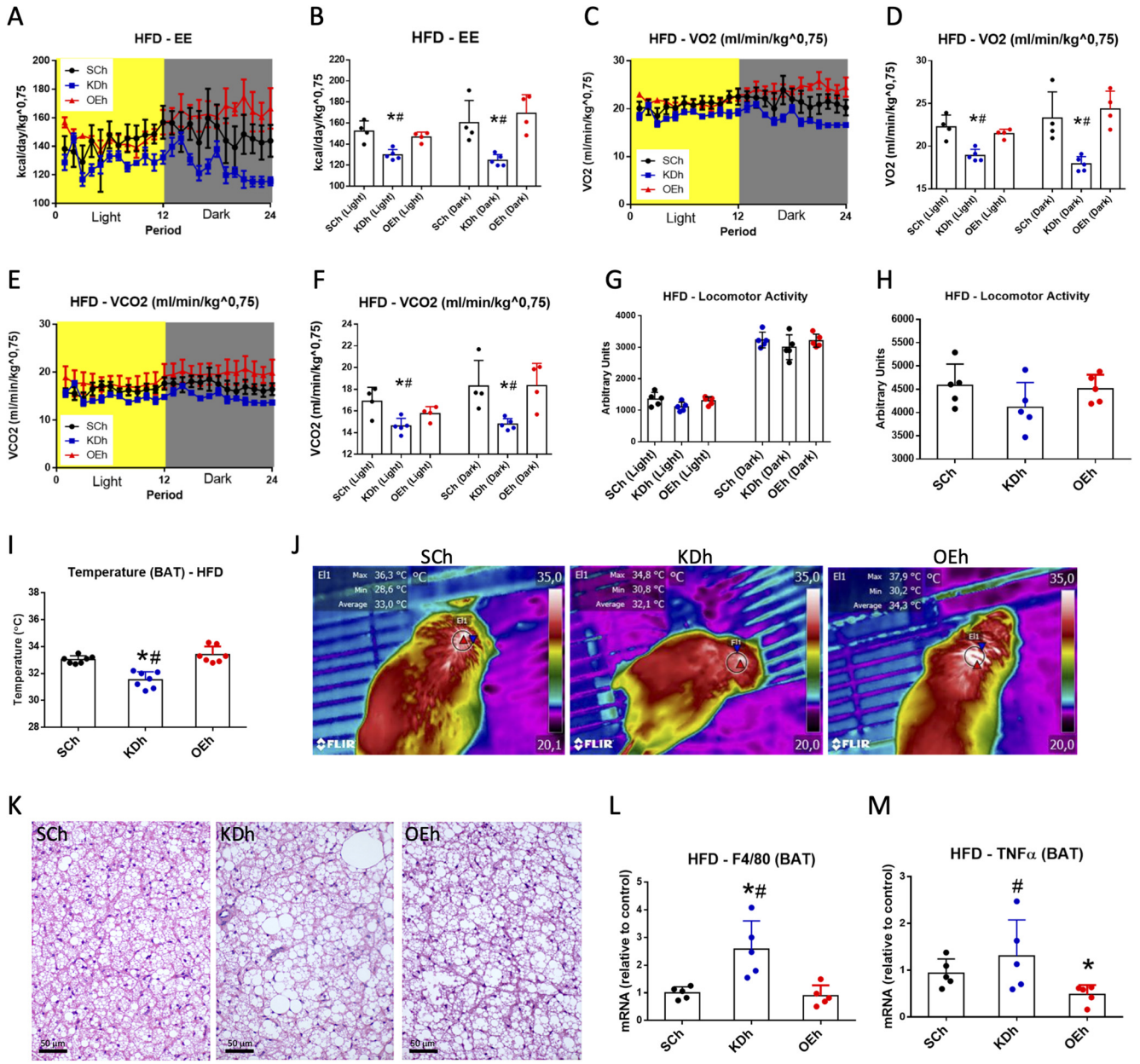

Figure 7. Energy expenditure and BAT parameters in mice under simultaneous introduction of an HFD and induction of overexpression of NHLH2 in the hypothalamus. Energy expenditure (***A***,***B***); oxygen consumption (***C***,***D***); carbon dioxide production (***E***,***F***); light- and dark-phase locomotor activity (***G***); whole-day locomotor activity (***H***); BAT temperature (***I***,***J***); BAT microscopic morphology (***K***); and BAT transcript expression of *Adgre1* (gene coding for F4/80) (***L***) and *Tnfa* (***M***) in mice submitted to the protocol depicted in Figure 6*E*. *$p < 0.05$ versus SCh. #$p < 0.05$ versus OEh. EE, Energy expenditure; KDh, knockdown fed an HFD; OEh, overexpression fed an HFD; SCh, scrambled fed an HFD. ***A-H***, ***K-M***, $n = 5$; ***I***, ***J***, $n = 7$. Mice fed on chow were also evaluated as shown in Extended Data Figure 7-1.

Table 4. Impact of Nhlh2 hypothalamic overexpression on body mass gain and caloric intake in female mice[a]

Parameter	SCc	OEc
Nhlh2 transcript (relative to control)	1.00 ± 0.32	1.38 ± 0.34*
Body mass gain (g)	9.4 ± 2.2	5.3 ± 2.0*
Caloric intake (kcal/d)	17.8 ± 3.3	13.1 ± 2.4*

[a]In all experiments, $n = 10$. SCc, Scrambled fed on chow; OEc, overexpression fed on chow.
*$p < 0.05$ versus SCc.

Table 5. Impact of Nhlh2 hypothalamic overexpression on sexual behavior and gonad size in female and male mice[a]

Parameter	SCc	OEc
Sexual behavior index	18.2 ± 9.3	19.7 ± 11.8
Ovary mass (mg)	11.2 ± 2.1	11.6 ± 2.5
Testis mass (mg)	9.8 ± 1.1	10.1 ± 1.4

[a]In all experiments, $n = 5$. SCc, Scrambled fed on chow; OEc, overexpression fed on chow.

targets), identifying 116 putative target genes for NHLH2 (Fig. 5*A*), including marker genes of TAC2/KISS1 and POMC neurons (Fig. 5*B*). The promoter regions from these genes were subsequently surveyed for the E-box motifs previously associated with NHLH2 binding with the purpose of validating such an approach. We found that only 8 of the 116 predicted target genes did not present these motifs within 1000 bp upstream of the TSS: *Tmem35*, *Nkx2.1*, *HQ.Q2*, *Fam159a*, *Tmem8c*, *Lrrc38*, *Gnai1*, and *X4932443I19Rik* (a proposed gene). Many of these

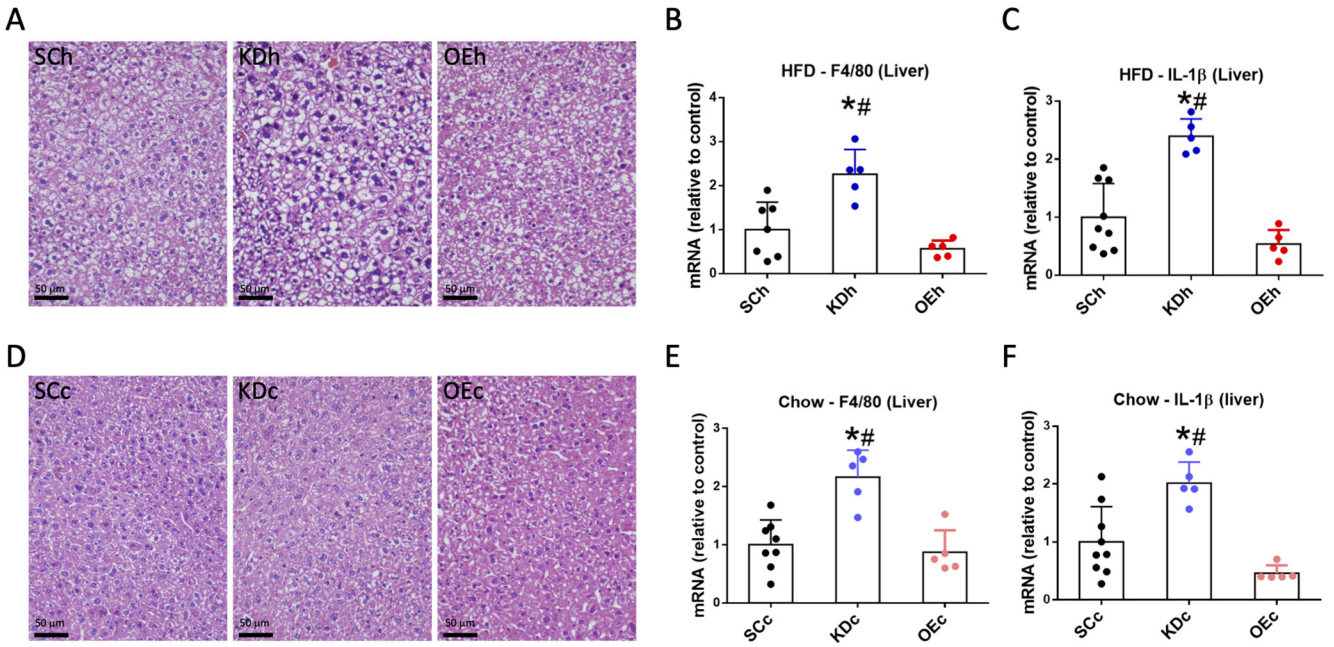

Figure 8. Liver histology and inflammatory markers in mice under simultaneous introduction of an HFD and induction of overexpression of NHLH2 in the hypothalamus. Liver histology of mice treated according to the protocol depicted in Figure 6*E* and fed on an HFD (***A***) or chow (***D***). Transcript expressions of *Adgre1* (gene coding for F4/80) (***B***,***E***) and *Il1b* (***C***,***F***) in the liver of mice treated according to the protocol depicted in Figure 6*E* and fed on an HFD (***B***,***C***) or chow (***E***,***F***). $^{*}p < 0.05$ versus scrambled (SCh or SCc, scrabbled fed on HFD or chow). $^{\#}p < 0.05$ versus overexpression (OEh or OEc, overexpression fed on HFD or chow). KD, Knockdown; KDc, knockdown fed on chow; KDh, knockdown fed on HFD; OE, overexpression; OEc, overexpression fed on chow; OEh, overexpression fed on HFD; SC, scrambled; SCc, scrabbled fed on chow; SCh, scrambles fed on HFD. In all experiments, $n = 5$-9.

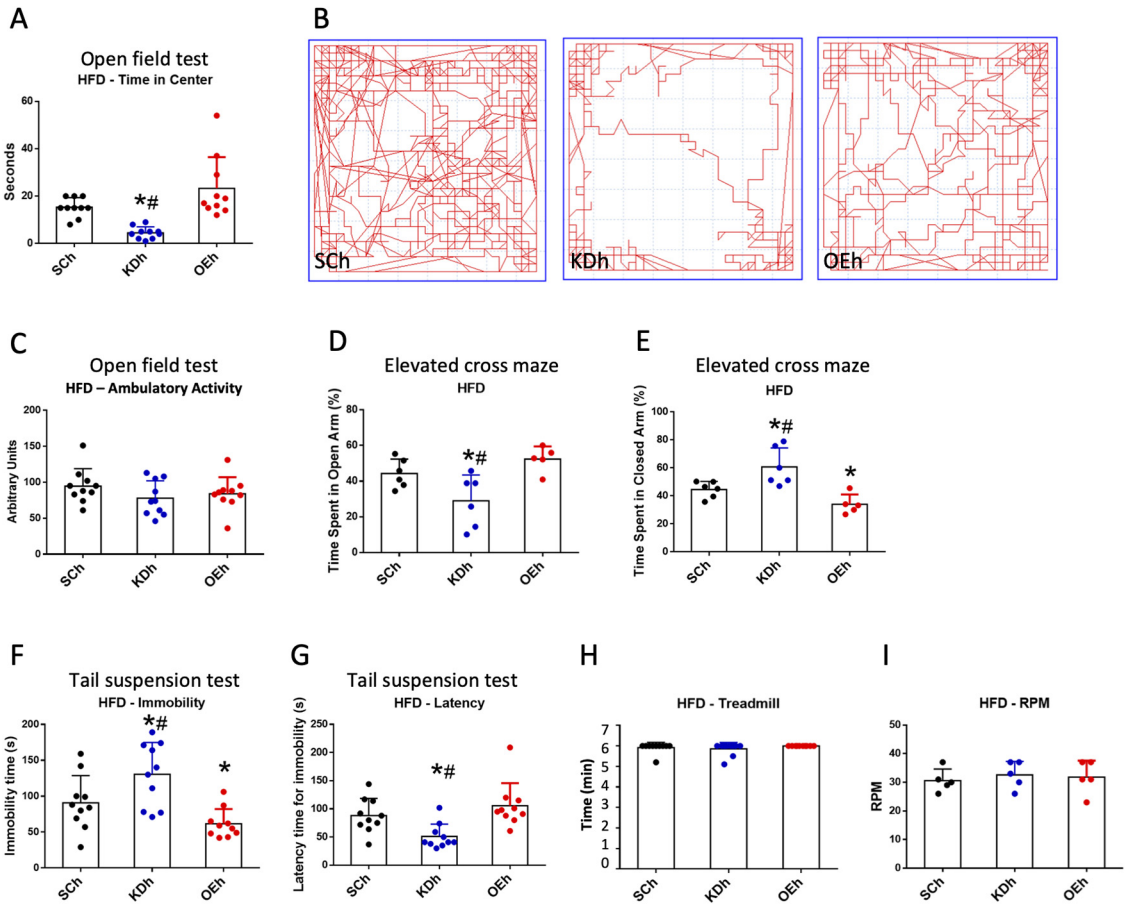

Figure 9. Behavioral changes induced by the overexpression of NHLH2 in the hypothalamus. Mice submitted to the protocol depicted in Figure 6*E* were evaluated in the open field test (***A-C***), elevated cross maze (***D***,***E***), tail suspension test (***F***,***G***), time spent on the treadmill (***H***), and maximum RPM in the rotarod test (***I***). $^{*}p < 0.05$ versus SCh. $^{\#}p < 0.05$ versus OEh. KDh, Knockdown fed an HFD; OEh, overexpression fed an HFD; SCh, scrambled fed an HFD. ***A-C***, ***F-H***, $n = 10$; ***D***, ***E***, ***I***, $n = 5$ or 6. Mice fed on chow were also evaluated as shown in Extended Data Figure 9-1.

downstream validated targets were also identified, presenting either direct or indirect correlation with *Nhlh2* in the hypothalamus of BXD mice (Fig. 5*C*). The functions of several important targets of NHLH2 identified by both approaches are listed in Table 3 and include genes involved in neuronal growth and differentiation, metabolism, the stress response, and neuroendocrine regulation.

Hypothalamic *Nhlh2* expression impacts on caloric intake and body mass

Next, we explored the impact of dietary factors and leptin on the hypothalamic expression of *Nhlh2*. As shown in Figure 6*A*, the consumption of an HFD induced a transient increase in the expression of hypothalamic *Nhlh2*, beginning 5 d after the diet intervention and lasting for 2 weeks; on prolonged feeding on an HFD, such as for 4 or 8 weeks, the levels of *Nhlh2* were similar to baseline. Refeeding (Fig. 6*B*) and exogenous leptin (Fig. 6*C*) also promoted increases in the hypothalamic expression of *Nhlh2*. Next, we tested lentiviruses aimed at inhibiting (KD) and increasing (OE) the expression of *Nhlh2*. The efficiencies of the lentiviruses were demonstrated in a cell-based system (Fig. 6*D*). Figure 6*E* depicts the design of the experiments presented in Figures 7-10, Tables 4 and 5, and Extended Data Figs 7-1 and 9-1. In mice fed chow (Fig. 6*F*) or an HFD (Fig. 6*G*), bilateral ARC injection of the lentiviruses into the ARC promoted significant inhibition or overexpression of *Nhlh2*; these changes were accompanied by concordant regulations of hypothalamic *Pcsk1* (Fig. 6*H*,*I*) and *Pomc* (Fig. 6*J*,*K*). Because the main objective of this study was to determine the impact of hypothalamic overexpression of NHLH2 on obesity, the remaining results represent the experiments performed with mice fed an HFD; however, all experiments were also performed with mice fed chow, and the results are presented in Extended Data Figs 7-1 and 9-1. In the initial set of experiments, the HFD was introduced shortly after mice received the intracerebroventricular injections of lentiviruses, which was intended to provide a model for obesity prevention. Under these settings, NHLH2 overexpression in the hypothalamus resulted in reduced caloric intake (Fig. 6*L*), reduced body mass gain (Fig. 6*M*,*N*), reduced adiposity (Fig. 6*O*,*P*), and reduced visceral adipose tissue adipocyte size (Fig. 6*Q*,*R*). Conversely, the inhibition of hypothalamic NHLH2 promoted significant increases in caloric intake (Fig. 6*L*), body mass gain (Fig. 6*M*,*N*), adiposity (Fig. 6*O*,*P*), and visceral adipose tissue adipocyte size (Fig. 6*Q*,*R*). The hypothalamic overexpression of NHLH2 was also effective to reduce caloric intake and body mass gain in female mice (Table 4).

The impact of hypothalamic NHLH2 expression on energy expenditure, BAT, and the liver

The hypothalamic overexpression of NHLH2 promoted no changes in energy expenditure (Fig. 7*A*,*B*), oxygen consumption (Fig. 7*C*,*D*), carbon dioxide production (Fig. 7*E*,*F*), spontaneous locomotor activity (Fig. 7*G*,*H*), BAT temperature (Fig. 7*I*,*J*), BAT microscopic morphology (Fig. 7*K*), and BAT F4/80 (*Adgre1*) expression (Fig. 7*L*). There was only a reduction in BAT *Tnfa* expression (Fig. 7*M*). Conversely, the inhibition of hypothalamic NHLH2 resulted in reduced energy expenditure (Fig. 7*A*,*B*), reduced oxygen consumption (Fig. 7*C*,*D*), reduced carbon dioxide production (Fig. 7*E*,*F*), reduced BAT temperature (Fig. 7*I*,*J*), increased size of fat droplets in BAT (Fig. 7*K*), and increased BAT F4/80 (*Adgre1*) expression (Fig. 7*L*). In the liver (Fig. 8), the hypothalamic overexpression of NHLH2 had no impact on the expression of inflammatory markers, whereas the inhibition of NHLH2 increased the expression of F4/80 (*Adgre1*) (Fig. 8*B*,*E*) and *Il1b* (Fig. 8*C*,*F*) transcripts.

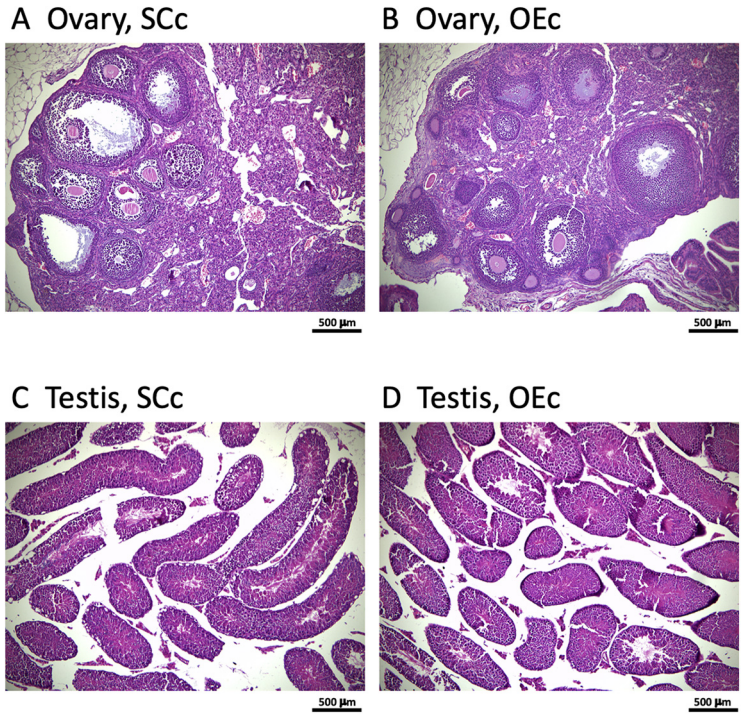

Figure 10. Gonad morphology under hypothalamic NHLH2 overexpression. Determination of ovary (***A***,***B***) and testis (***C***, ***D***) histologic aspect in mice submitted to NHLH2 hypothalamic overexpression. OEc, Overexpression fed on chow; SCc, scrambled fed on chow. Images are representative of three independent experiments.

The impact of hypothalamic NHLH2 expression on behavior

It was previously shown that NHLH2 activates monoamine oxidase A (*Maoa*) gene transcription, resulting in decreased serotonin levels and the emergence of an anxiety/depression-like phenotype (Libert et al., 2011). Here, we confirmed that inhibition of NHLH2 promoted behavioral changes that are compatible with the anxiety/depression-like phenotype. Thus, in the open field test, mice spent a shorter time in the center of the field, whereas total ambulatory activity was preserved (Fig. 9*A*–*C*). In the elevated cross maze, mice spent a shorter time in the open arm (Fig. 9*D*,*E*); and in the tail suspension test, mice spent a longer time immobile and had a shorter latency (Fig. 9*F*,*G*). When hypothalamic NHLH2 expression was increased, there was an improvement in the obesity-associated anxiety/depression-like phenotype: Mice spent less time in the closed arm of the elevated cross maze (Fig. 9*E*) and had a shorter latency in the tail suspension test (Fig. 9*F*). None of these findings were affected by physical capacity, as there were no changes in the treadmill and rotarod tests for either inhibition or overexpression of hypothalamic NHLH2 (Fig. 9*H*,*I*). In addition, the hypothalamic overexpression of NHLH2 affected neither sexual behavior (Table 5) nor gonad size (Table 5) nor gonad morphology (Fig. 10).

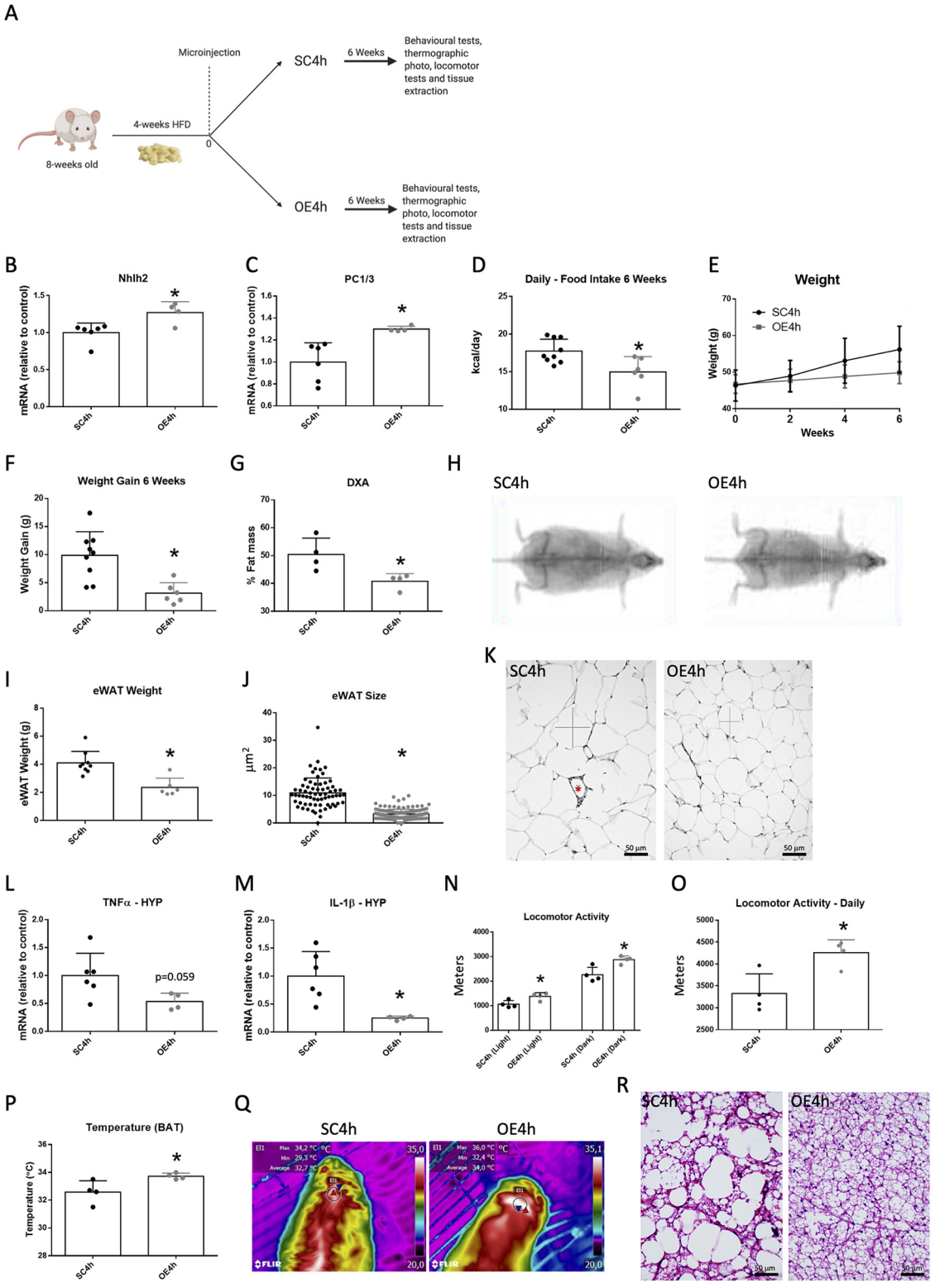

Figure 11. Reduction of body mass gain in obese mice submitted to overexpression of NHLH2 in the hypothalamus. ***A***, Schematic representation of the protocols used for evaluation of the impact of modulating hypothalamic NHLH2 in diet-induced obese mice that were introduced to an HFD 4 weeks before the lentivirus injections, the obesity treatment model. Transcript expressions of *Nhlh2* (***B***) and *Pcsk1* (gene coding for PC1/3) (***C***). Food intake (***D***), body mass (***E***), body mass gain during the 6 week intervention (***F***), adiposity as determined using DEXA (***G***,***H***), epididymal white adipose tissue mass (***I***), and mean epididymal white adipocyte size (***J***,***K***). Transcripts for *Tnfa* and *Il1b* were determined in the hypothalamus of mice (***L***,***M***). Light- and dark-phase locomotor activity (***N***), whole day locomotor activity (***O***), BAT temperature (***P***,***Q***), and BAT microscopic morphology (***R***). *$p < 0.05$ versus SC4h. ***K***, Red asterisk represents crown-like structures. Crossed lines indicate measurement of adipocyte areas. DXA, Dual X-ray absorptiometry; eWAT, epididymal white adipose tissue; HYP, hypothalamus; OE, overexpression; OE4h, overexpression fed an HFD for 4 weeks before lentivirus injections and maintained on an HFD thereafter until the end of the experimental period; SC, scrambled; SC4h, scrambled fed an HFD for 4 weeks before lentivirus injection and maintained on an HFD thereafter until the end of the experimental period. ***B***, ***C***, ***L***, ***M***, $n = 6$; ***D-F***, ***I***, $n = 6$-9; ***G***, ***H***, ***N-R***, $n = 4$.

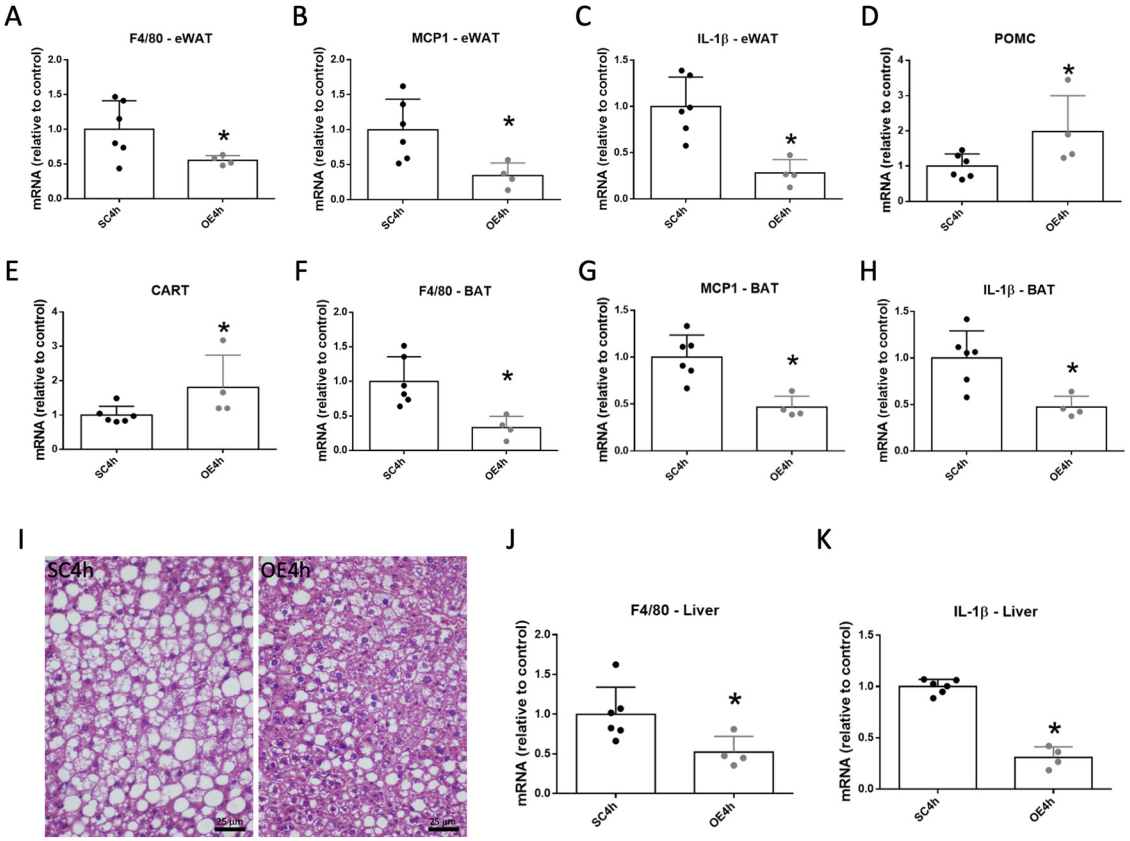

Figure 12. The phenotype of obese mice submitted to overexpression of NHLH2 in the hypothalamus. In mice submitted to the protocol depicted in Figure 11*A*, the transcript expressions of *Adgre1* (gene coding for F4/80) (***A***), *Ccl2* (gene coding for MCP1) (***B***), and *Il1b* (***C***) were determined in the epididymal white adipose tissue; the transcript expressions of *Pomc* (***D***) and *Cart* (***E***) were determined in the hypothalamus; the transcripts of *Adgre1* (gene coding for F4/80) (***F***), *Ccl2* (gene coding for MCP1) (***G***), and *Il1b* (***H***) were determined in the BAT; liver histology is depicted in ***I***, and the transcripts of *Adgre1* (gene coding for F4/80) (***J***) and *Il1b* (***K***) were determined in the liver. *$p < 0.05$ versus SC4h. eWAT, Epididymal white adipose tissue; OE, overexpression; OE4h, overexpression fed on HFD for 4 weeks before lentivirus injection and maintained on HFD thereafter until the end of the experimental period; SC, scrambled; SC4h, scrambled fed on HFD for 4 weeks before lentivirus injection and maintained on HFD thereafter until the end of the experimental period. In al experiments, $n = 5$ or 6.

The impact of overexpressing NHLH2 in the hypothalamus of previously obese mice

Figure 11*A* depicts the approach used in experiments presented in Figures 11-13. In this approach, mice were fed an HFD for 4 weeks before lentivirus injection bilaterally in the ARC; this protocol was aimed at providing an experimental setting for treating obesity. The bilateral injection of the overexpression (OE4h) lentivirus promoted a 30% increase in the expressions of *Nhlh2* (Fig. 11*B*) and *Pcsk1* (Fig. 11*C*) in the hypothalamus. This was accompanied by reduced caloric intake (Fig. 11*D*), reduced body mass gain (Fig. 11*E*,*F*), reduced adiposity (Fig. 11*G*,*H*), reduced epididymal adipose tissue mass (Fig. 11*I*), and reduced mean epididymal adipocyte size (Fig. 11*J*,*K*). The expression of inflammatory markers was reduced in the adipose tissue (Fig. 12*A*,*C*). In addition, there were reductions in hypothalamic expression of *Tnfa* and *Il1b* (Fig. 11*L*,*M*) and increased expression of *Pomc* and *Cart* (Fig. 12*D*,*E*). Obese mice with increased hypothalamic expression of NHLH2 presented with increased spontaneous locomotor activity (Fig. 11*N*,*O*), increased BAT temperature (Fig. 11*P*,*Q*), and a reduction in BAT lipid droplet size (Fig. 11*R*). This was accompanied by reduced expression of inflammatory markers in the BAT (Fig. 12*F*–*H*). In the liver, the inhibition of hypothalamic NHLH2 resulted in reduced steatosis and reduced expression of inflammatory markers (Fig. 12*I*–*K*).

Behavioral outcomes of inhibiting hypothalamic NHLH2 in obesity

The increased hypothalamic expression of NHLH2 impacted behavior beneficially, reducing the anxiety/depression-like phenotype (Fig. 13*A*–*H*), as demonstrated by increased time spent in the center of the open field test (Fig. 13*A*,*B*) and reduced time to immobility in the tail suspension test (Fig. 13*F*). This was not accompanied by changes in physical capacity (Fig. 13*H*,*I*), but it was accompanied by increased spontaneous ambulatory activity (Fig. 13*C*).

Discussion

NHLH2 was first characterized for its role in the development of the CMS and retina (Brown et al., 1992; Gobel et al., 1992; Li et al., 2001). This was confirmed by the germline deletion of the *Nhlhl2* gene, revealing that the development of the hypothalamic-pituitary axis is particularly affected and leads to an obese and hypogonadal phenotype (Good et al., 1997), and by the retroviral-induced misexpression of *Nhlh2* in the retina that promotes retinal degeneration (Li et al., 2001). Subsequent studies have shown that mice lacking *Nhlh2* present with reduced spontaneous physical activity, which contributes to the development of obesity, preceding increased caloric intake and reduced energy expenditure (Coyle et al., 2002). Despite robust evidence suggesting that NHLH2 could be an attractive target for the treatment of obesity, no previous study has evaluated the impact of its

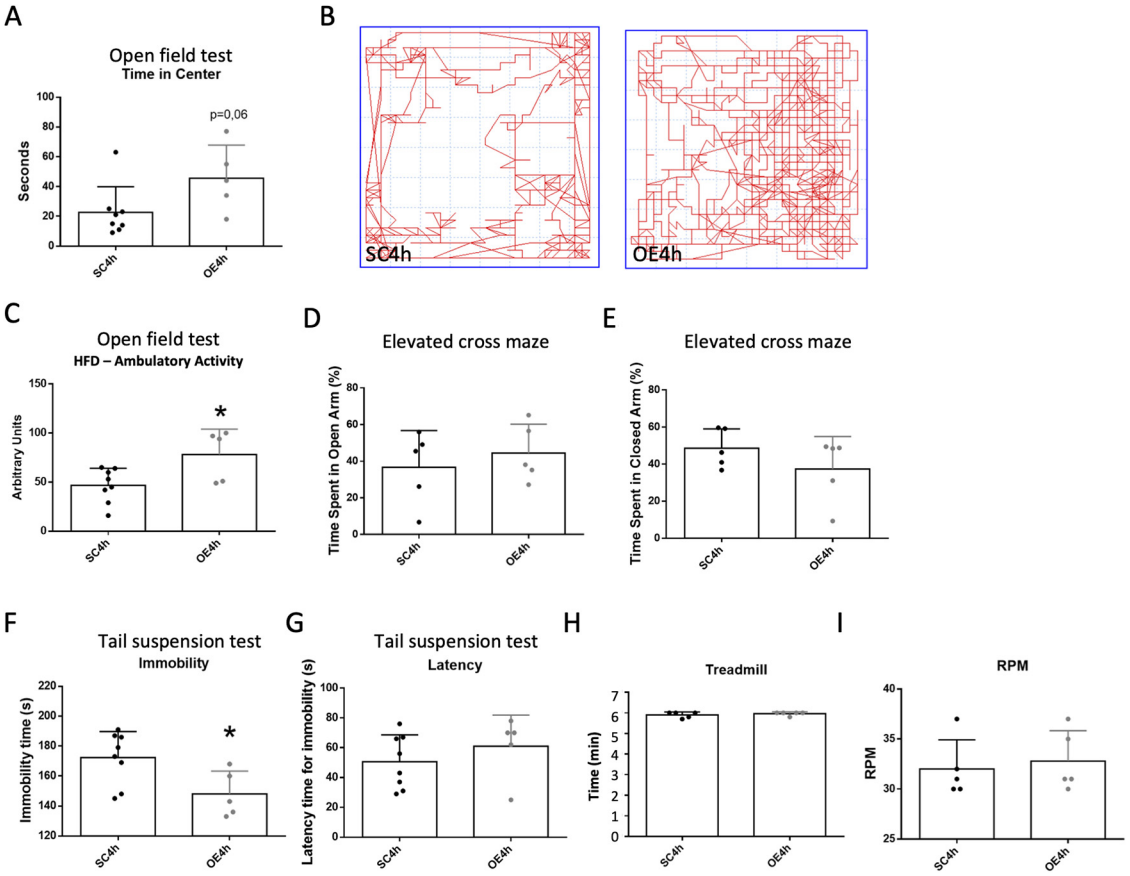

Figure 13. Behavioral changes induced by the overexpression of NHLH2 in the hypothalamus of obese mice. Mice submitted to the protocol depicted in Figure 11*A* were evaluated in the open field test (***A-C***), elevated cross maze (***D,E***), tail suspension test (***F,G***), time spent on the treadmill (***H***), and maximum RPM in the rotarod test (***I***). $^{*}p < 0.05$ versus SC4h. $^{\#}p < 0.05$ versus OE4h. OE, Overexpression; OE4h, overexpression fed an HFD for 4 weeks before lentivirus injection and maintained on an HFD thereafter until the end of the experimental period; SC, scrambled; SC4h, scrambled fed an HFD for 4 weeks before lentivirus injection and maintained on an HFD thereafter until the end of the experimental period. In all experiments, $n = 5$-8.

overexpression in experimental obesity. Here, we showed that NHLH2 overexpression in the ARC is sufficient to prevent and treat DIO.

In the first part of the study, we analyzed the transcriptomes of 20,000+ ARC single cells to determine the identity of cells expressing *Nhlh2* in this region. Previous studies using histologic methods have reported the expression of *Nhlh2* in POMC and GnRH neurons (Kruger et al., 2004; Cogliati et al., 2007; Schmid et al., 2007; Vella et al., 2007), and at least four studies have reported the expression of *Nhlh2* transcripts in POMC neurons using scRNAseq approaches (Henry et al., 2015; Huisman et al., 2019; Haddad-Tóvolli et al., 2020; Shi et al., 2020). However, none of the previous scRNAseq studies used a search strategy centered on the presence of *Nhlh2* transcripts. Here, we asked what ARC cells express *Nhlh2* and showed that only neurons, mostly POMC and KISS1, express this transcript.

Next, we used two distinct strategies to identify potential transcriptional targets for NHLH2: the analysis of transcriptional networks by *arboreto* (Aibar et al., 2017; Van de Sande et al., 2020) and the analysis of the BXD mice families (Andreux et al., 2012). There was a considerable overlap of targets identified by either method, a finding that could be regarded as evidence of specificity for the methods. Some of the targets were previously known, such as *Pomc* and *Pcsk1* (Jing et al., 2004; Schmid et al., 2013); however, there were new targets identified by both methods that could contribute to further understanding the roles of NHLH2 in obesity, behavior, and reproduction. This is particularly true for LIM homeobox 5 (*Lhx5*), which is involved in neuronal differentiation and reproductive regulation in the hypothalamus (Granger et al., 2006; Burgess, 2007); nuclear receptor Subfamily 5 Group A Member 2 (*Nr5a2*), which is involved in hyperphagia associated with the use of antipsychotic drugs (Perez-Gomez et al., 2018); nuclear receptor Subfamily 4 Group A Member 2 (*Nr4a2*), which is involved in the regulation of dopaminergic systems, POMC expression, and attention deficit behavior (Montarolo et al., 2019; Huggett and Stallings, 2020; Jiang et al., 2020); and amyloid β precursor protein (*App*), which is involved in the development of Alzheimer's disease, a condition related to obesity and diabetes (Clarke et al., 2015; Cavadas et al., 2016).

To promote NHLH2 overexpression, we used a lentivirus that was injected bilaterally into the ARC. We also used a lentivirus designed to inhibit NHLH2; this was used as a control because the phenotype obtained by the inhibition of NHLH2 has been studied extensively (Coyle et al., 2002; Jing et al., 2004; Schmid et al., 2013). Using this approach, we obtained a consistent impact on the expression of NHLH2, which resulted in parallel regulations of the target genes *Pomc* and *Pcsk1*. The transcriptional regulation of hypothalamic *Pomc* is complex and depends on several transcription factors. The details of this regulation have been recently reviewed previously (Rubinstein and Low, 2017). NHLH2 can directly regulate *Pomc*, but most of the regulatory action occurs indirectly via *Pcsk1*. Thus, unlike STAT3, which is directly involved in *Pomc* transcriptional regulation, experimental modifications of NHLH2 expression could result in distinct impacts on POMC levels, depending on the model studied.

Regarding the phenotypic outcomes, we asked whether the hypothalamic overexpression of NHLH2 could prevent the development of DIO. To explore this topic, an HFD was introduced simultaneously with the injection of the lentiviruses into the hypothalami of mice. In this experimental setting, NHLH2 overexpression resulted in reduced body mass gain, mostly because of the reduction of caloric intake. In a separate set of experiments, we also evaluated the impact of NHLH2 overexpression in lean mice; and under physiological conditions, the NHLH2 overexpression did not impact on caloric intake and body mass. Studies have shown that, during the early development of DIO, the increase in caloric intake explains the first phase of body mass gain (Souza et al., 2016; Razolli et al., 2020). After prolonged exposure to an HFD, caloric intake returns to normality and obesity is maintained by a combination of changes in other components of the energy homeostasis machinery, such as thermogenesis, physical activity, and the gut microbiota (Almeida et al., 1996; Mozes et al., 2008; Fleissner et al., 2010; Sefcikova et al., 2010; Guo and Hall, 2011; Souza et al., 2016; Razolli et al., 2020). Because the increased hypothalamic expression of NHLH2 impacts on PC1/3 and POMC, we propose that the preventive effect of early overexpression of NHLH2 relies mostly on the central control of feeding. As body mass gain is prevented, the other abnormalities impacting on energy homeostasis that eventually occur in obesity are blunted.

To further explore the impact of overexpressing hypothalamic NHLH2 in experimental obesity, we injected the lentiviruses in obese mice that were fed on an HFD for 4 weeks. In this scenario, in addition to reducing caloric intake, the intervention promoted an increase in BAT temperature and an increase in physical activity. The involvement of NHLH2 in the regulation of spontaneous physical activity has been reported in studies characterizing the phenotype of whole-body *Nhlh2* KO (Coyle et al., 2002; Good et al., 2008). Mice devoid of *Nhlh2* from conception had a 50% reduction in physical activity (Good et al., 2008), and because this phenotype is present early in life, researchers suggested that it could impact on obesity predisposition earlier than changes in caloric intake and thermogenesis (Coyle et al., 2002). Another important mechanism of action of NHLH2 in the regulation of body energy homeostasis occurs by controlling the adrenergic inputs to the white and BAT depots, therefore regulating thermogenesis (Wankhade et al., 2010). Importantly, in all previous studies evaluating the roles of NHLH2 in energy homeostasis, only KO or inhibition of *Nhlh2* had been studied. Here, we have provided the first evidence for an important role for NHLH2 overexpression as a mechanism to regulate body mass beneficially in the context of experimental obesity.

An additional phenotypic change induced by the hypothalamic overexpression of NHLH2 relies on the reduction of the anxiety/depression-like behavior. This was evident both in the preventive and therapeutic models. It was previously shown that NHLH2 is targeted by the deacetylase SIRT1, increasing its transcriptional activity toward the *Maoa* promoter and therefore reducing brain serotonin levels (Libert et al., 2011). In addition, in humans, there is considerable evidence supporting the association between obesity and anxiety/depression, which is regarded as an important component of the overfeeding phenotype (Gariepy et al., 2010; Jebeile et al., 2019). Because of the existence of potential confounding factors, defining behavioral phenotypes can be optimized by the analysis of a combination of methods (Walsh and Cummins, 1976). Here, we used four different methods that in combination validated the model and, in addition, showed the beneficial impact of NHLH2 overexpression, reducing the anxiety/depression-like behavior. Of note, in the therapeutic model shown in Figure 13, the increased ambulatory activity of mice under NHLH2 overexpression could be a confounding factor for the interpretation of the open field test; however, the attenuation of the anxiety/depression-like behavior is supported by the reduced time of immobility in the tail suspension test. Thus, NHLH2 emerges as a potential therapeutic target that simultaneously regulates body mass and obesity-associated anxiety/depression-like behavior.

A weakness of this study is the fact that the intervention was not cell-specific; rather, it was restricted anatomically to the ARC. However, as demonstrated in the scRNAseq data, *Nhlh2* is expressed predominantly in POMC and KISS1 neurons; thus, the results reported herein may reflect changes in the activity of NHLH2 mostly in these subpopulations of neurons.

In conclusion, we have shown that the hypothalamic overexpression of NHLH2 can either prevent or treat experimental obesity. In the case of prevention, the outcome relies mostly on the reduction of caloric intake, whereas in the case of treatment, it results from a combined action on caloric intake, thermogenesis, and physical activity. Another important aspect related to the hypothalamic overexpression of NHLH2 is its beneficial impact on behavior. NHLH2 overexpression promoted a reduction of the anxiety/depression-like behavior both in the preventative and therapeutic models, which raises additional interest in this target, considering the common clinical association between obesity and anxiety/depression.

References

Ahituv N, Kavaslar N, Schackwitz W, Ustaszewska A, Martin J, Hebert S, Doelle H, Ersoy B, Kryukov G, Schmidt S, Yosef N, Ruppin E, Sharan R, Vaisse C, Sunyaev S, Dent R, Cohen J, McPherson R, Pennacchio LA (2007) Medical sequencing at the extremes of human body mass. Am J Hum Genet 80:779–791.

Ahlenius S, Larsson K (1984) Apomorphine and haloperidol-induced effects on male rat sexual behavior: no evidence for actions due to stimulation of central dopamine autoreceptors. Pharmacol Biochem Behav 21:463–466.

Aibar S, Gonzalez-Blas CB, Moerman T, Huynh-Thu VA, Imrichova H, Hulselmans G, Rambow F, Marine JC, Geurts P, Aerts J, van den Oord J, Atak ZK, Wouters J, Aerts S (2017) SCENIC: single-cell regulatory network inference and clustering. Nat Methods 14:1083–1086.

Al Rayyan N, Wankhade UD, Bush K, Good DJ (2013) Two single nucleotide polymorphisms in the human nescient helix-loop-helix 2 (NHLH2) gene reduce mRNA stability and DNA binding. Gene 512:134–142.

Al Rayyan N, Zhang J, Burnside AS, Good DJ (2014) Leptin signaling regulates hypothalamic expression of nescient helix-loop-helix 2 (Nhlh2) through signal transducer and activator 3 (Stat3). Mol Cell Endocrinol 384:134–142.

Almeida NG, Levitsky DA, Strupp B (1996) Enhanced thermogenesis during recovery from diet-induced weight gain in the rat. Am J Physiol 271: R1380–R1387.

Andreux PA, Williams EG, Koutnikova H, Houtkooper RH, Champy MF, Henry H, Schoonjans K, Williams RW, Auwerx J (2012) Systems genetics of metabolism: the use of the BXD murine reference panel for multiscalar integration of traits. Cell 150:1287–1299.

Becht E, McInnes L, Healy J, Dutertre CA, Kwok IW, Ng LG, Ginhoux F, Newell EW (2018) Dimensionality reduction for visualizing single-cell data using UMAP. Nat Biotechnol 37:38–44.

Brown L, Espinosa R 3rd, Le Beau MM, Siciliano MJ, Baer R (1992) HEN1 and HEN2: a subgroup of basic helix-loop-helix genes that are coexpressed in a human neuroblastoma. Proc Natl Acad Sci USA 89:8492–8496.

Bumaschny VF, Yamashita M, Casas-Cordero R, Otero-Corchón V, de Souza FS, Rubinstein M, Low MJ (2012) Obesity-programmed mice are rescued by early genetic intervention. J Clin Invest 122:4203–4212.

Burgess D (2007) Taking on that first faculty job. Nature 447:1142.

Burnett LC, LeDuc CA, Sulsona CR, Paull D, Rausch R, Eddiry S, Carli JF, Morabito MV, Skowronski AA, Hubner G, Zimmer M, Wang L, Day R, Levy B, Fennoy I, Dubern B, Poitou C, Clement K, Butler MG, Rosenbaum M, et al. (2017) Deficiency in prohormone convertase PC1 impairs prohormone processing in Prader–Willi syndrome. J Clin Invest 127:293–305.

Butler A, Hoffman P, Smibert P, Papalexi E, Satija R (2018) Integrating single-cell transcriptomic data across different conditions, technologies, and species. Nat Biotechnol 36:411–420.

Campbell JN, Macosko EZ, Fenselau H, Pers TH, Lyubetskaya A, Tenen D, Goldman M, Verstegen AM, Resch JM, McCarroll SA, Rosen ED, Lowell BB, Tsai LT (2017) A molecular census of arcuate hypothalamus and median eminence cell types. Nat Neurosci 20:484–496.

Cavadas C, Aveleira CA, Souza GF, Velloso LA (2016) The pathophysiology of defective proteostasis in the hypothalamus: from obesity to ageing. Nat Rev Endocrinol 12:723–733.

Clarke JR, Lyra E Silva NM, Figueiredo CP, Frozza RL, Ledo JH, Beckman D, Katashima CK, Razolli D, Carvalho BM, Frazão R, Silveira MA, Ribeiro FC, Bomfim TR, Neves FS, Klein WL, Medeiros R, LaFerla FM, Carvalheira JB, Saad MJ, Munoz DP, et al. (2015) Alzheimer-associated Abeta oligomers impact the central nervous system to induce peripheral metabolic deregulation. EMBO Mol Med 7:190–210.

Cogliati T, Delgado-Romero P, Norwitz ER, Guduric-Fuchs J, Kaiser UB, Wray S, Kirsch IR (2007) Pubertal impairment in Nhlh2 null mice is associated with hypothalamic and pituitary deficiencies. Mol Endocrinol 21:3013–3027.

Coyle CA, Jing E, Hosmer T, Powers JB, Wade G, Good DJ (2002) Reduced voluntary activity precedes adult-onset obesity in Nhlh2 knockout mice. Physiol Behav 77:387–402.

da Silva AA, do Carmo JM, Hall JE (2020) CNS regulation of glucose homeostasis: role of the leptin-melanocortin system. Curr Diab Rep 20:29.

Festing MF, Altman DG (2002) Guidelines for the design and statistical analysis of experiments using laboratory animals. ILAR J 43:244–258.

Fleissner CK, Huebel N, Abd El-Bary MM, Loh G, Klaus S, Blaut M (2010) Absence of intestinal microbiota does not protect mice from diet-induced obesity. Br J Nutr 104:919–929.

Fox DL, Good DJ (2008) Nescient helix-loop-helix 2 interacts with signal transducer and activator of transcription 3 to regulate transcription of prohormone convertase 1/3. Mol Endocrinol 22:1438–1448.

Gariepy G, Nitka D, Schmitz N (2010) The association between obesity and anxiety disorders in the population: a systematic review and meta-analysis. Int J Obes (Lond) 34:407–419.

Gobel V, Lipkowitz S, Kozak CA, Kirsch IR (1992) NSCL-2: a basic domain helix-loop-helix gene expressed in early neurogenesis. Cell Growth Differ 3:143–148.

Good DJ, Porter FD, Mahon KA, Parlow AF, Westphal H, Kirsch IR (1997) Hypogonadism and obesity in mice with a targeted deletion of the Nhlh2 gene. Nat Genet 15:397–401.

Good DJ, Coyle CA, Fox DL (2008) Nhlh2: a basic helix-loop-helix transcription factor controlling physical activity. Exerc Sport Sci Rev 36:187–192.

Granger A, Bleux C, Kottler ML, Rhodes SJ, Counis R, Laverriere JN (2006) The LIM-homeodomain proteins Isl-1 and Lhx3 act with steroidogenic factor 1 to enhance gonadotrope-specific activity of the gonadotropin-releasing hormone receptor gene promoter. Mol Endocrinol 20:2093–2108.

Guo J, Hall KD (2011) Predicting changes of body weight, body fat, energy expenditure and metabolic fuel selection in C57BL/6 mice. PLoS One 6: e15961.

Haddad-Tóvolli R, Altirriba J, Obri A, Sánchez EE, Chivite I, Milà-Guasch M, Ramírez S, Gómez-Valadés AG, Pozo M, Burguet J, Velloso LA, Claret M (2020) Pro-opiomelanocortin (POMC) neuron translatome signatures underlying obesogenic gestational malprogramming in mice. Mol Metab 36:100963.

Hafemeister C, Satija R (2019) Normalization and variance stabilization of single-cell RNA-seq data using regularized negative binomial regression. Genome Biol 20:296.

Henry FE, Sugino K, Tozer A, Branco T, Sternson SM (2015) Cell type-specific transcriptomics of hypothalamic energy-sensing neuron responses to weight-loss. Elife 4:e09800.

Hinney A, Schmidt A, Nottebom K, Heibult O, Becker I, Ziegler A, Gerber G, Sina M, Gorg T, Mayer H, Siegfried W, Fichter M, Remschmidt H, Hebebrand J (1999) Several mutations in the melanocortin-4 receptor gene including a nonsense and a frameshift mutation associated with dominantly inherited obesity in humans. J Clin Endocrinol Metab 84:1483–1486.

Huggett SB, Stallings MC (2020) Genetic architecture and molecular neuropathology of human cocaine addiction. J Neurosci 40:5300–5313.

Huisman C, Cho H, Brock O, Lim SJ, Youn SM, Park Y, Kim S, Lee SK, Delogu A, Lee JW (2019) Single cell transcriptome analysis of developing arcuate nucleus neurons uncovers their key developmental regulators. Nat Commun 10:3696.

Huszar D, Lynch CA, Fairchild-Huntress V, Dunmore JH, Fang Q, Berkemeier LR, Gu W, Kesterson RA, Boston BA, Cone RD, Smith FJ, Campfield LA, Burn P, Lee F (1997) Targeted disruption of the melanocortin-4 receptor results in obesity in mice. Cell 88:131–141.

Jebeile H, Gow ML, Baur LA, Garnett SP, Paxton SJ, Lister NB (2019) Association of pediatric obesity treatment, including a dietary component, with change in depression and anxiety: a systematic review and meta-analysis. JAMA Pediatr 173:e192841.

Jiang L, Wei H, Yan N, Dai S, Li J, Qu L, Chen X, Guo M, Chen Z, Chen Y (2020) Structural basis of NR4A1 bound to the human pituitary proopiomelanocortin gene promoter. Biochem Biophys Res Commun 523:1–5.

Jing E, Nillni EA, Sanchez VC, Stuart RC, Good DJ (2004) Deletion of the Nhlh2 transcription factor decreases the levels of the anorexigenic peptides alpha melanocyte-stimulating hormone and thyrotropin-releasing hormone and implicates prohormone convertases I and II in obesity. Endocrinology 145:1503–1513.

Kent WJ, Sugnet CW, Furey TS, Roskin KM, Pringle TH, Zahler AM, Haussler D (2002) The human genome browser at UCSC. Genome Res 12:996–1006.

Krude H, Biebermann H, Luck W, Horn R, Brabant G, Gruters A (1998) Severe early-onset obesity, adrenal insufficiency and red hair pigmentation caused by POMC mutations in humans. Nat Genet 19:155–157.

Kruger M, Ruschke K, Braun T (2004) NSCL-1 and NSCL-2 synergistically determine the fate of GnRH-1 neurons and control necdin gene expression. EMBO J 23:4353–4364.

Kuhnen P, Krude H, Biebermann H (2019) Melanocortin-4 receptor signalling: importance for weight regulation and obesity treatment. Trends Mol Med 25:136–148.

Lewis S (1991) An esthetic titanium abutment: report of a technique. Int J Oral Maxillofac Implants 6:195–201.

Li CM, Yan RT, Wang SZ (2001) Atrophy of Muller glia and photoreceptor cells in chick retina misexpressing cNSCL2. Invest Ophthalmol Vis Sci 42:3103–3109.

Libert S, Pointer K, Bell EL, Das A, Cohen DE, Asara JM, Kapur K, Bergmann S, Preisig M, Otowa T, Kendler KS, Chen X, Hettema JM, van den Oord EJ, Rubio JP, Guarente L (2011) SIRT1 activates MAO-A in the brain to mediate anxiety and exploratory drive. Cell 147:1459–1472.

Montarolo F, Martire S, Perga S, Spadaro M, Brescia I, Allegra S, De Francia S, Bertolotto A (2019) NURR1 deficiency is associated to ADHD-like phenotypes in mice. Transl Psychiatry 9:207.

Moraes JC, Coope A, Morari J, Cintra DE, Roman EA, Pauli JR, Romanatto T, Carvalheira JB, Oliveira AL, Saad MJ, Velloso LA (2009) High-fat diet induces apoptosis of hypothalamic neurons. PLoS One 4:e5045.

Mozes S, Bujnakova D, Sefcikova Z, Kmet V (2008) Developmental changes of gut microflora and enzyme activity in rat pups exposed to fat-rich diet. Obesity (Silver Spring) 16:2610–2615.

Pellow S, Chopin P, File SE, Briley M (1985) Validation of open:closed arm entries in an elevated plus-maze as a measure of anxiety in the rat. J Neurosci Methods 14:149–167.

Perez-Gomez A, Carretero M, Weber N, Peterka V, To A, Titova V, Solis G, Osborn O, Petrascheck M (2018) A phenotypic *Caenorhabditis elegans* screen identifies a selective suppressor of antipsychotic-induced hyperphagia. Nat Commun 9:5272.

Razolli DS, de Araujo TM, Sant Apos Ana MR, Kirwan P, Cintra DE, Merkle FT, Velloso LA (2020) Proopiomelanocortin processing in the hypothalamus is directly regulated by saturated fat: implications for the development of obesity. Neuroendocrinology 110:92–104.

Rubinstein M, Low MJ (2017) Molecular and functional genetics of the proopiomelanocortin gene, food intake regulation and obesity. FEBS Lett 591:2593–2606.

Schmid T, Kruger M, Braun T (2007) NSCL-1 and -2 control the formation of precerebellar nuclei by orchestrating the migration of neuronal precursor cells. J Neurochem 102:2061–2072.

Schmid T, Gunther S, Mendler L, Braun T (2013) Loss of NSCL-2 in gonadotropin releasing hormone neurons leads to reduction of pro-opiomelanocortin neurons in specific hypothalamic nuclei and causes visceral obesity. J Neurosci 33:10459–10470.

Sefcikova Z, Kmet V, Bujnakova D, Racek L, Mozes S (2010) Development of gut microflora in obese and lean rats. Folia Microbiol (Praha) 55:373–375.

Shi R, Shan C, Duan X, Chen Z, Liu P, Song J, Song T, Bi X, Han C, Wu L, Gao G, Hu X, Zhang Y, Tong Z, Huang W, Liu WJ, Wu G, Zhang B, Wang L, Qi J, et al. (2020) A human neutralizing antibody targets the receptor-binding site of SARS-CoV-2. Nature 584:120–124.

Souza GF, Solon C, Nascimento LF, De-Lima-Junior JC, Nogueira G, Moura R, Rocha GZ, Fioravante M, Bobbo V, Morari J, Razolli D, Araujo EP, Velloso LA (2016) Defective regulation of POMC precedes hypothalamic inflammation in diet-induced obesity. Sci Rep 6:29290.

Strauss BE, Patricio JR, de Carvalho AC, Bajgelman MC (2006) A lentiviral vector with expression controlled by E2F-1: a potential tool for the study and treatment of proliferative diseases. Biochem Biophys Res Commun 348:1411–1418.

Van de Sande B, Flerin C, Davie K, De Waegeneer M, Hulselmans G, Aibar S, Seurinck R, Saelens W, Cannoodt R, Rouchon Q, Verbeiren T, De Maeyer D, Reumers J, Saeys Y, Aerts S (2020) A scalable SCENIC workflow for single-cell gene regulatory network analysis. Nat Protoc 15:2247–2276.

Vella KR, Burnside AS, Brennan KM, Good DJ (2007) Expression of the hypothalamic transcription factor Nhlh2 is dependent on energy availability. J Neuroendocrinol 19:499–510.

Walsh RN, Cummins RA (1976) The Open-Field Test: a critical review. Psychol Bull 83:482–504.

Wankhade UD, Good DJ (2011) Melanocortin 4 receptor is a transcriptional target of nescient helix-loop-helix-2. Mol Cell Endocrinol 341:39–47.

Wankhade UD, Vella KR, Fox DL, Good DJ (2010) Deletion of Nhlh2 results in a defective torpor response and reduced beta adrenergic receptor expression in adipose tissue. PLoS One 5:e12324.

Yi CX, Walter M, Gao Y, Pitra S, Legutko B, Kälin S, Layritz C, García-Cáceres C, Bielohuby M, Bidlingmaier M, Woods SC, Ghanem A, Conzelmann KK, Stern JE, Jastroch M, Tschöp MH (2017) TNFalpha drives mitochondrial stress in POMC neurons in obesity. Nat Commun 8:15143.